Model predictive maneuvering control and energy management for all-electric autonomous ships

Haseltalab, Ali; Negenborn, Rudy R.

DOI
10.1016/j.apenergy.2019.113308

Publication date
2019

Document Version
Final published version

Published in
Applied Energy

Citation (APA)
Haseltalab, A., & Negenborn, R. R. (2019). Model predictive maneuvering control and energy management for all-electric autonomous ships. *Applied Energy*, *251*, Article 113308. https://doi.org/10.1016/j.apenergy.2019.113308

Applied Energy 251 (2019) 113308

Contents lists available at ScienceDirect

Applied Energy

journal homepage: www.elsevier.com/locate/apenergy

Model predictive maneuvering control and energy management for all-electric autonomous ships

Ali Haseltalab*, Rudy R. Negenborn

Department of Maritime and Transport Technology, Delft University of Technology, Delft, the Netherlands

HIGHLIGHTS

- State space models are proposed for all-electric ships.
- Novel predictive energy management and maneuvering control approaches are proposed.
- Using the approaches, optimal engine loading is guaranteed.
- The fuel efficiency increases by 2–15% depending on the operating profile.
- Trajectory tracking performance is improved.

ARTICLE INFO

Keywords:
Autonomous ships
Model predictive control
Energy management
All-electric DC power and propulsion system

ABSTRACT

Over the last few years, autonomous shipping has been under extensive investigation by the scientific community where the main focus has been on ship maneuvering control and not on the optimal use of energy sources. In this paper, the purpose is to bridge the gap between maneuvering control, energy management, and the control of the Power and Propulsion System (PPS) to improve fuel efficiency and the performance of the vessel. Maneuvering control, energy management, and the control of the PPS are in the literature typically studied independently from one another, while they are closely connected. A generic control methodology based on receding horizon control techniques is proposed for the ship maneuvering control as well as energy management. In the context of this research, Direct Current (DC) all-electric architectures are considered for the PPS where the relationship between the produced power by energy sources and vessel propellers is established by a DC microgrid. The objective of the proposed approach is to ensure the ship mission objectives by guaranteeing efficient power availability, decreasing the trajectory tracking error, and increasing the fuel efficiency. In this regard, for the ship motion control, a Model Predictive Control (MPC) algorithm is proposed which is based on Input–Output Feedback Linearization (IOFL). Through this algorithm, the required power for the ship mission is predicted and then, transferred to the proposed Predictive Energy Management (PEM) algorithm which decides on the optimal split between different on-board energy sources during the mission. As a result, the fuel efficiency and the power system stability can be increased. Several simulations are carried out for the evaluation of the proposed approach. The results suggest that by adopting the proposed approach, the trajectory tracking error decreases and the Specific Fuel Consumption (SFC) efficiency is significantly improved.

1. Introduction

The concept of autonomous shipping, its benefits, and future utilization are undergoing extensive study and investigation by both academic and industrial communities. Autonomous ships are expected to yield advantage from several points of view such as reduced crew cost, higher safety, and more adaptability to different operating profiles. However, several challenges need to be addressed before fully operational autonomous ships can be enabled. These difficulties include problems with automatic path planning, navigation and trajectory tracking, cooperation with other vessels, power and energy management issues, and fault-detection, isolation and reconfiguration. To address these issues, several researches have been and being carried out in academia and maritime industries. Path planning approaches are designed with obstacle avoidance

* Corresponding author at: Delft University of Technology, Faculty of 3ME, Department of Maritime and Transport Technology, Building 34, Mekelweg 2, 2628CD Delft, the Netherlands.
E-mail addresses: a.haseltalab@tudelft.nl (A. Haseltalab), r.r.negenborn@tudelft.nl (R.R. Negenborn).

https://doi.org/10.1016/j.apenergy.2019.113308
Received 1 March 2019; Received in revised form 3 May 2019; Accepted 8 May 2019

features to steer the vessel in congested waterways based on the specifications and dynamics of the vessel [1]and also to increase fuel efficiency during operation [2]. Novel navigation and trajectory tracking approaches are proposed to steer the ship smoothly towards its planned trajectory in congested waterways [3] and also in the presence of uncertainties [4]. Cooperation of autonomous ships has recently been considered for path following with collision avoidance capabilities [5,6] and also for platooning and building vessel train formations [7]. Energy management issues have been addressed to increase the fuel efficiency [8,9] and robustness of the on-board power system [10] while also increasing the autonomy of the power and propulsion system. In unmanned vessels fault-detection, isolation and reconfiguration is a vital issue [11]. These problems have been considered in the literature for both the electric power system [12] and also propulsion system of vessels [13]. Due to the expected reduced number of on-board crew members in autonomous vessels the role for automation and independent machine performance in all of the mentioned issues increases significantly and becomes more vital. For this purpose, the adoption of intelligent control and management algorithms for diverse purposes is necessary.

Alongside with increased autonomy, and mainly due to environmental restrictions from international maritime authorities, there is a shift towards more efficient Power and Propulsion System (PPS) architectures as a replacement for direct-diesel propulsion configurations [8]. As a result, the complexity of the on-board PPS architecture is increasing due to the addition of several components such as synchronous generators, induction motors, and power conversion modules. Furthermore, it has been proved that such advanced architectures cannot be as efficient as expected unless advanced control and energy management algorithms are adopted [8,9]. These architectures can be divided into two different types: *hybrid* architectures where the relationship between diesel engine and propellers is established directly and also through electrical machinery [8,14] and *all-electric* architectures where this relationship is formed only through an electrical grid [15,16]. There have been several research works for increasing the fuel efficiency of ships with these architectures. For more information regarding these works see [8,17] and references therein.

1.1. DC power and propulsion systems

Among different architectures, in this paper, the focus is on the DC Power and Propulsion System (DC-PPS) architecture which, with advances in the domain of semiconductors, is perceived as one of the most efficient architectures [17]. Several advantages of DC-PPS are the possibility for optimal engine loading, variable diesel engine speed, and fuel efficiency, which make this PPS suitable for ships with different operational profiles. Moreover, increase of flexibility in the design stage and a decrease in the number of converting stages are among advantages of DC on-board microgrids [15,8]. As a result, DC-PPS can be a proper power system candidate for autonomous ships. On the other hand, there are several challenges in taking full advantage of this architecture such as power system stability [18], fault tolerance [12], and optimal energy management issues [17]. As a result, the complexity of this architecture suggests performing more elaborate investigations to increase the performance and efficiency of this architecture. In [15], an on-board DC-PPS is modeled and the interaction between different components are investigated. This work is extended in [17] where an energy management algorithm is proposed to increase fuel efficiency under different loading conditions. In [10,19], MPC-based algorithms are used for energy management where a combination of ultra-capacitors and a battery is adopted for on-board energy storage.

To guarantee power availability during operation, the energy management controller should cooperate with maneuvering controller. This cooperation should be devised in a form of information exchange where the future required power for the operation is predicted within a finite horizon and made available for the energy management controller to guarantee power availability during the operation.

1.2. Maneuvering control

The problem of maneuvering control of autonomous vessels in the presence of environmental disturbances is one of the main challenges on the way of having fully autonomous ships. Intelligent controllers of autonomous ships should be capable of propelling the vessel towards an apriory planned path. Regardless of difficulties within controlling this complex system, one of the main issues is to keep the ship as close as possible to the planned trajectory in the presence of environmental disturbances such as waves and currents. This issue exposes its significance in or near port areas and hinterlands where the problem of waterway congestion exists. The problem of trajectory tracking control is being studied extensively, where several approaches have been proposed for the trajectory tracking control including Model Predictive Control (MPC) [3,20], adaptive schemes [21,22] and nonlinear methods [23,20]. In [3], a linear Model Predictive Control (MPC) algorithm is proposed to address the problem of trajectory tracking control with knowledge over arrival time where the nonlinear model of the vessel is linearized to decrease computational complexity. Nonlinear MPC schemes are adopted in [20] for trajectory tracking in the presence of uncertainties. A neural learning control strategy is adopted in [24] to guarantee trajectory tracking of an autonomous vessel with uncertainties within its model. In [25], the trajectory tracking problem is investigated using neural-adaptive control schemes in the existence of output constraints and parameter uncertainties in the maneuvering model. Maneuvering control in the presence of uncertainties within propeller's model is considered in [4] where an adaptive control approach is proposed for trajectory tracking. These control strategies are extended to multi-vessel applications where different vessels should collaborate with each other to fulfill diverse tasks including trajectory tracking [26] and platooning [7]. However, in none of the above works the interaction between the PPS and the ship maneuvering control algorithm is considered.

1.3. Contributions of the paper

In this paper, the objective is to bridge the gap between maneuvering control on one hand and energy management on the other hand to maximize the fuel efficiency of the all-electric vessels and improve their performance. First, the overall system is described and a mathematical model is presented for different components. A mathematical model in 3 Degrees of Freedom (3DoF) is presented for the vessel which captures the vessel's voyage in waterways. Moreover, the overall DC-PPS is modeled and a benchmark is created for experimenting the proposed approaches. Then, an MPC algorithm is proposed for the purpose of trajectory tracking and maneuvering control. The MPC algorithm is designed based on Input–Output Feedback Linearization (IOFL) that is established by using the results in [27,28]. By adopting this technique, quadratic programming methods can be applied for solving the optimization problem which leads to a significant decrease in computational costs. Then, using the propeller dynamics and the efficiency curve of induction motors [9], the predicted required power is estimated over a finite horizon. This estimation is used for determining the optimal power split between different energy sources on-board, where the objective is to maximize the fuel efficiency and contribute to the robustness of the power system by avoiding sudden changes in diesel-generator's loading condition. The energy management algorithm guarantees that if a Diesel-Generator-Rectifier (DGR)

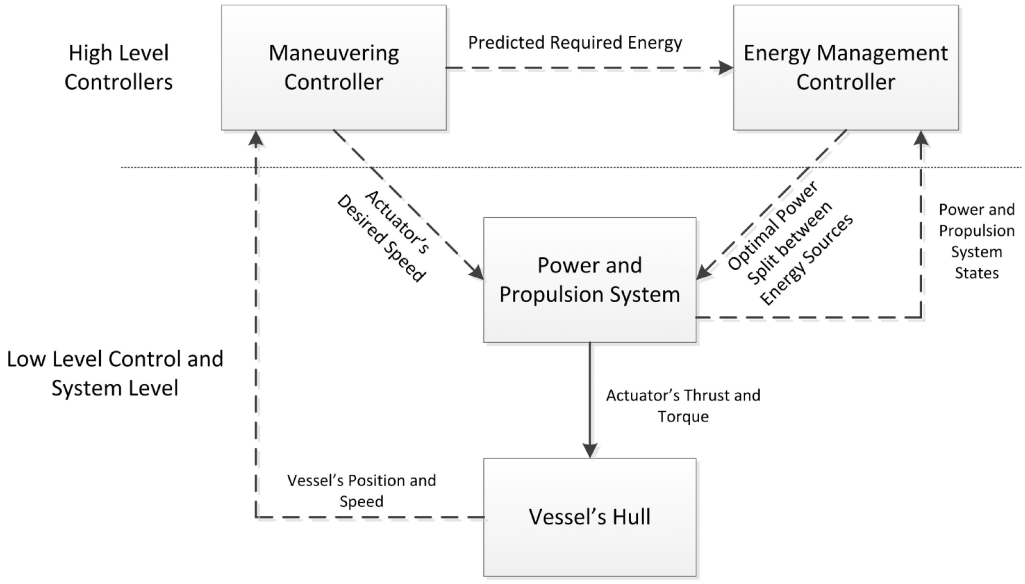

Fig. 1. Block diagram of the proposed control methodology.

set is in-line, it functions around its optimal point in Specific Fuel Consumption (SFC) curve. This is achieved by determining an optimal split between DGR sets and the battery. Using this so-called Predictive Energy Management (PEM) approach, the battery's power is used for damping the load fluctuations. In Fig. 1, the block diagram of the proposed control methodology is presented. All in all, the contributions of the paper are:

1. Modeling the overall ship with DC-PPS and representing its mathematical model in a state-space format.
2. Proposing an MPC approach for maneuvering control of the vessel in 3DoF which is designed by adopting IOFL and linearization of constraints so that quadratic programming approaches can be adopted.
3. Through the proposed predictive maneuvering control approach, the future required energy for the ship operation is predicted in a finite horizon and is used by the energy management controller.
4. An energy management approach is proposed which guarantees the optimal power split between different energy sources by taking into account the predicted required energy, the objective is to increase the SFC efficiency during operation.

For evaluation of the proposed control approaches, several simulations are carried out including a trajectory tracking simulation in the port of Rotterdam and operating profiles of real harbor tugs. It is shown that the trajectory tracking error is decreased and fuel efficiency is increased if the proposed generic approach is adopted.

1.4. Outline

The remainder of the paper is organized as follows. In Section 2, the ship maneuvering model and the overall DC-PPS are described. In Section 3, the MPC algorithm for the motion control of autonomous ships is presented. In Section 4, the proposed PEM approach is described and its interactions with the motion control algorithm is described. The results of simulations are presented in Section 6. In Section 7, concluding remarks and future research directions are provided.

2. System description

In this section, the overall system under study is described. First, the equations of motion in 3DoF are presented for the maneuvering model of the vessel. Then, the DC-PPS architecture is explained and a mathematical model for each of its components is given. The maneuvering model dynamics represent the lowest block (vessel's hull) and DC-PPS is power and propulsion system block in Fig. 1.

2.1. 3DoF maneuvering model

In the context of this paper, the 3DoF motion of the ship is considered [23,22]. The maneuvering model of the ship can then be described as:

$$\begin{aligned} &\dot{\eta}_s(t) = R(\eta_s(t))v_s(t) \\ &M_s\dot{v}_s(t) + C_s(v_s(t))v_s(t) = \tau_s(t) + \tau_{\text{drag}}(v_s(t), \eta_s(t)), \end{aligned} \tag{1}$$

where $\eta_s(t) = [x(t), y(t), r(t)]^T$ is the ship position and orientation at time t, $v_s(t) = [v_x(t), v_y(t), v_r(t)]^T$ is the 3DoF ship speed and τ_s is the vector of forces applied to the ship center of gravity. M_s is the Inertial Mass matrix which consists of rigid body and added mass matrices.

$$M_s = M_{RB} + M_A \tag{2}$$

where

$$M_s = \begin{bmatrix} m_b & 0 & 0 \\ 0 & m_b & 0 \\ 0 & 0 & I_z \end{bmatrix}, \quad M_A = \begin{bmatrix} m_{ax} & 0 & 0 \\ 0 & m_{ay} & 0 \\ 0 & 0 & I_a \end{bmatrix}. \tag{3}$$

Parameter m_b is the mass of the vessel, I_z is the moment of inertia, m_{ax} and m_{ay} are the added mass in x and y direction, respectively, and I_a represents the added moment of inertia.

Matrix $C_s(\cdot)$ is the Coriolis and Centrifugal matrix defined as:

$$C_s(v_s) = \begin{bmatrix} 0 & 0 & -mv_y \\ 0 & 0 & mv_x \\ mv_y & -mv_x & 0 \end{bmatrix}. \tag{4}$$

Function $\tau_{\text{drag}}(.)$, which is a function of ship speed and course angle, represents drag forces in 3DoF applied to the craft. The details of this function are provided in appendix.

Matrix $R(\eta_s)$ is a Jacobian matrix that transforms ship velocity from body-fixed into inertial velocities, defined as:

$$R(\eta_s) = \begin{bmatrix} \cos(r) & -\sin(r) & 0 \\ \sin(r) & \cos(r) & 0 \\ 0 & 0 & 1 \end{bmatrix}. \tag{5}$$

Vector τ_s is the vector of forces generated by propellers applied to the ship center of gravity and is:

$$\tau_s(t) = \begin{bmatrix} \tau_x(t) \\ \tau_y(t) \\ \tau_r(t) \end{bmatrix} \tag{6}$$

where τ_x and τ_y are surge and sway forces and τ_r is the yaw moment.

Considering non-rotatable typical propellers, the relationship between the thrust produced by actuators (propellers and thrusters) and the vector of forces is [23]:

$$\tau_s = \Gamma_{3\times m} \begin{bmatrix} g_1(n_1) \\ \vdots \\ g_m(n_m) \end{bmatrix}, \tag{7}$$

where g_1, ...,g_m are actuator dynamics, n_1, ...,n_m are actuators shaft speeds, m is the number of actuators, and Γ is the thrust configuration matrix defined as:

$$\Gamma = [\gamma_1 \ \cdots \ \gamma_m], \tag{8}$$

with γ_1, γ_2, ...,γ_m column vectors for standard actuators. If the actuator is a propeller, then:

$$\gamma_i = \begin{bmatrix} 1 \\ 0 \\ -l_y \end{bmatrix}; \tag{9}$$

if the actuator is a stern or bow thruster, then:

$$\gamma_i = \begin{bmatrix} 0 \\ 1 \\ l_x \end{bmatrix}, \tag{10}$$

where l_y and l_x represent the position of the actuator in the vessel's reference frame. Since, generally, Γ is not a square matrix the solution to the problem of unconstrained thrust allocation to non-rotatable actuators can be found using the pseudo-inverse of Γ:

$$\tau_{ac} = \Gamma^{\mathrm{T}}(\Gamma\Gamma^{T})^{-1}\tau_s. \tag{11}$$

2.2. DC power and propulsion system

The fulfillment of the ship desired operation is not only dependent on the ship maneuvering control algorithm but it is also vitally related to power availability during the operation. As a result, the PPS should be studied alongside to the ship maneuvering model. In this paper, a DC-PPS is considered for the vessel.

On-board DC microgrids consist of prime-mover(s) and AC/DC conversion modules on the energy generation side and motor controller inverters, induction motors, propellers and other loads (like hotel loads, weaponry facilities, etc) on the consumption side. Diesel-generator sets act as prime-movers. The generators are connected to six-pulse rectifiers where the AC/DC conversion process is carried out. The DGR sets are connected to the consumption side through a DC-link which in our study consists of a capacitor. The schematic of the system under study is shown in Fig. 2. Note that for redundancy and safety purposes in some variations of this architecture, more than one bus bar exist.

One of the main advantages of DC-PPS is enabling the use of variable speed generators. As a result, the diesel engine can run at variable speed which can lead to a reduction in fuel consumption [8]. This feature alongside with the other benefits of this architecture (mentioned in the introduction) increases the flexibility of this PPS which leads to increased adaptability to different operating profiles. On the other hand, one of the major challenges for enabling the DC-PPS is the problem of stability. In the context of this paper, the stability problem is addressed form an energy management point of view where the proposed approach guarantees the power availability and prohibits DGR sets to undergo extreme and rapid changes in their loading condition by prioritizing the battery when the energy generation side faces rapid load transients.

The consumption side of DC-PPS contains induction motors that are connected to propellers and thrusters as well as non-propulsive loads such as hotel loads. The induction motors are connected to the DC bus using motor controller inverters. In the remainder of this section, a mathematical model is given for the different components of the DC-PPS.

2.2.1. Propeller

The relationship between the shaft speed and propeller torque and thrust is established using the following equations [29]:

$$T_{\mathrm{p}} = K_{\mathrm{T}}\rho D^4 |n_{\mathrm{p}}| n_{\mathrm{p}} \tag{12}$$

$$Q_{\mathrm{p}} = K_{\mathrm{Q}}\rho D^5 |n_{\mathrm{p}}| n_{\mathrm{p}}, \tag{13}$$

where D is the propeller diameter and ρ is the water density. Parameters K_{T} and K_{Q} are thrust and torque coefficients which are functions of propeller structure and advance ratio J_{p}[30] that is:

$$J_{\mathrm{p}} = \frac{V_{\mathrm{a}}}{n_{\mathrm{p}} D}$$

where V_{a} is the advance speed of the ship.

2.2.2. Induction motor

The model of the induction motor is also represented in the dq-reference frame [31]. The dynamical equations of the squirrel-cage machine are:

$$\begin{aligned} \dot{\psi}_{\mathrm{dsm}} &= v_{\mathrm{dsm}} - \omega_{\mathrm{p}}\psi_{\mathrm{qsm}} + r_{\mathrm{sm}} i_{\mathrm{dsm}} \\ \dot{\psi}_{\mathrm{qsm}} &= v_{\mathrm{qsm}} - \omega_{\mathrm{p}}\psi_{\mathrm{dsm}} - r_{\mathrm{sm}} i_{\mathrm{qsm}} \\ \dot{\psi}_{\mathrm{drm}} &= v_{\mathrm{drm}} + (\tfrac{2}{p}\omega_{\mathrm{p}} - \omega_{\mathrm{e}})\psi_{\mathrm{qrm}} - r_{\mathrm{rm}} i_{\mathrm{drm}} \\ \dot{\psi}_{\mathrm{qrm}} &= v_{\mathrm{qrm}} - (\tfrac{2}{p}\omega_{\mathrm{p}} - \omega_{\mathrm{e}})\psi_{\mathrm{drm}} - r_{\mathrm{rm}} i_{\mathrm{qrm}} \\ Q_{\mathrm{em}} &= 1.5p(\psi_{\mathrm{dsm}} i_{\mathrm{qsm}} - \psi_{\mathrm{qsm}} i_{\mathrm{dsm}}), \end{aligned} \tag{14}$$

where i_{dsm} and i_{qsm} are stator currents in the dq-reference frame, i_{drm} and i_{qrm} are rotor currents, ψ_{dsm}, ψ_{qsm}, ψ_{drm} and ψ_{qrm} are the stator and rotor fluxes, respectively. Parameter p represents the number of poles, ω_{p} is the rotor speed, ω_{e} is the electrical angular velocity and Q_{em} is the electric torque. The stator and rotor voltages in the dq-frame are shown as v_{dsm}, v_{qsm}, v_{drm} and v_{qrm}, respectively. The relationship between the machine currents and fluxes are established using the machine inductances L_{sm}, L_{rm} and L_{mm} as:

$$\begin{aligned} \psi_{\mathrm{qsm}} &= L_{\mathrm{sm}} i_{\mathrm{qsm}} + L_{\mathrm{mm}} i_{\mathrm{qrm}} \\ \psi_{\mathrm{dsm}} &= L_{\mathrm{sm}} i_{\mathrm{dsm}} + L_{\mathrm{mm}} i_{\mathrm{drm}} \\ \psi_{\mathrm{qrm}} &= L_{\mathrm{rm}} i_{\mathrm{qrm}} + L_{\mathrm{mm}} i_{\mathrm{qsm}} \\ \psi_{\mathrm{drm}} &= L_{\mathrm{rm}} i_{\mathrm{drm}} + L_{\mathrm{mm}} i_{\mathrm{dsm}}. \end{aligned} \tag{15}$$

A voltage source inverter is used as a converting stage between the DC-link and the machine which controls the machine by adopting a

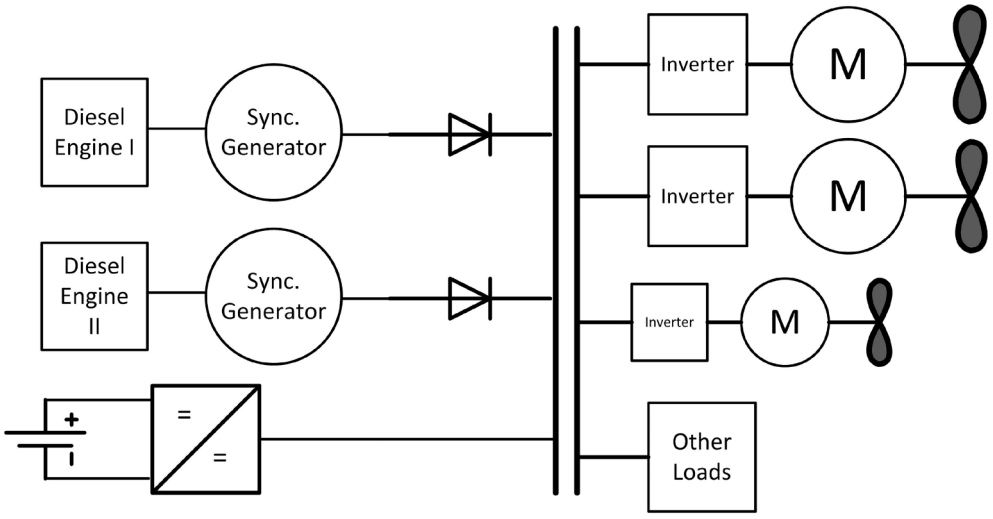

Fig. 2. The DC-PPS under study.

direct torque control technique [31].

2.2.3. Diesel engine

The diesel engine is the primary energy supplier by transforming chemical energy to mechanical energy. The produced power appears as torque generation. The diesel engine dynamics can be approximated by nonlinear or linear equations (see, e.g., [29,32,33]), depending on the level of accuracy needed. In this paper, a linear model is adopted to accommodate the relationship between the fuel index and produced torque Q_{en} by means of a transfer function as below [34]:

$$\dot{Q}_{en} = -\frac{Q_{en}}{\tau_{en}} + K_{en} f_{en}, \tag{16}$$

where K_{en} is the torque constant, f_{en} is the governor setting (i.e., fuel index and flow) and τ_{en} is the torque buildup constant which determines the response speed of the diesel engine, a function of diesel-generator shaft speed:

$$\tau_{en} = \frac{0.9}{\omega_{dg}}, \tag{17}$$

where ω_{dg} represents the rotational speed [35].

2.2.4. Synchronous generator

The mechanical energy is transformed to electrical energy by use of the synchronous generators. The relationship between a generator and a diesel engine is established through the shaft speed where the generated torque of the diesel engine is an input for the generator. In the context of this research, the Park equivalent Direct-Quadratic (dq) modeling approach is used to represent the dynamics of the synchronous generator. The relationship between the voltages, fluxes, and currents in the dq reference frame is established using the following equations:

$$\begin{aligned}
\dot{\psi}_d &= -v_d + \omega_{dg}\psi_q + r_s i_d \\
\dot{\psi}_q &= -v_q + \omega_{dg}\psi_d + r_s i_q \\
\dot{\psi}_{fd} &= v_{fd} - r_{fd} i_{fd} \\
\dot{\psi}_{kd} &= -r_{kd} i_{kd} \\
\dot{\psi}_{kq} &= -r_{kq} i_{kq},
\end{aligned} \tag{18}$$

where r_s, r_{fd}, r_{kd}, and r_{kq} are stator, field circuit and damping resistances, respectively. Variables ψ_d and ψ_q are fluxes in the d and q axis, ψ_{kd} and ψ_{kq} are damper fluxes; field flux is represented by ψ_{fd}. In the above model, v_d and v_q are dq voltages and v_{fd} is the field voltage of the generator. The mechanical dynamics of the synchronous generator are given as:

$$\dot{\omega}_{dg} = \frac{1}{2H}(\psi_d i_q - \psi_q i_d + Q_{en}), \tag{19}$$

where ω_{dg} is the shaft speed of the diesel generator, Q_{en} is the mechanical torque produced by the diesel engine, and $H = \frac{J}{p}$ is the inertia constant per pole. Using the system inductances, the relationship between electrical currents and fluxes can be established as:

$$\begin{bmatrix} i_d \\ i_q \\ i_{fd} \\ i_{kd} \\ i_{kq} \end{bmatrix} = \begin{bmatrix} -L_d & 0 & L_{md} & L_{md} & 0 \\ 0 & -L_q & 0 & 0 & L_{mq} \\ -L_{md} & 0 & L_{fd} & L_{md} & 0 \\ -L_{md} & 0 & L_{md} & L_{kd} & 0 \\ 0 & -L_{mq} & 0 & 0 & L_{kq} \end{bmatrix}^{-1} \begin{bmatrix} \psi_d \\ \psi_q \\ \psi_{fd} \\ \psi_{kd} \\ \psi_{kq} \end{bmatrix} \tag{20}$$

where L_d, L_{md}, L_{kd}, L_{fd}, L_q, L_{mq} and L_{kq} are per unit inductances ([31]).

2.2.5. Rectifier and the DC-link

We consider an average value model with constant parameters is considered for the uncontrollable rectifier [36]. In our model, the rectifier is introduced to the benchmark with generator currents as input and DC current as the output. The DC current can be computed as:

$$i_{dc} = \beta_{rec}\sqrt{i_q^2 + i_d^2}. \tag{21}$$

The DC-link voltage is derived using the below Kirchhoff equation:

$$\dot{v}_{dc} = \frac{1}{C}(i_{dc} - i_{load}) \tag{22}$$

where i_{load} is the DC load current.

The dq-voltages from the rectifier to the generator are as follows:

$$\begin{aligned}
v_q &= \alpha_{rec} v_{dc} \cos(\theta_g) \\
v_d &= \alpha_{rec} v_{dc} \sin(\theta_g),
\end{aligned} \tag{23}$$

where θ_g is the load angle and is computed as below:

$$\theta_g = \arctan(\frac{i_d}{i_q}) - \phi_{rec}. \tag{24}$$

Variables α_{rec}, β_{rec} and ϕ_{rec} are considered constant in this model.

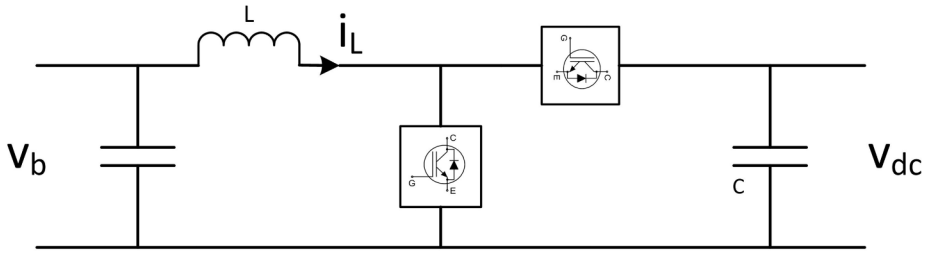

Fig. 3. The architecture of the non-isolated converter.

2.2.6. Battery

A model from [37] is used for representing the battery dynamics. This is suitable for power and energy management purposes. The State-of-Charge (SoC) of the battery is determined using:

$$S_{oC}(k+1) = S_{oC}(k) - \left(\frac{\eta_i \Delta t}{C_n}\right) i_b \tag{25}$$

where η_i is the cell Coulombic efficiency, i.e., $\eta_i = 1$ for discharge and $\eta_i \leqslant 1$ for charge. Parameter C_n is the nominal capacity of the battery, k is the sampling time, Δt is the sampling period, and i_b is the battery current. The battery voltage can be derived as:

$$v_b = O_{CV}(SoC(k)) - r_b i_b \tag{26}$$

where O_{CV} is the open circuit voltage of the battery and is a function of S_{oC} and r_b is the battery resistance.

2.2.7. Bidirectional converter

A non-isolated bidirectional converter is considered for the DC-PPS. Non-isolated bidirectional converters are suitable for low and medium voltage DC microgrids. They are cheaper and have lower losses compared to isolated converters. The configuration of the non-isolated bidirectional converter considered for this paper is illustrated in Fig. 3.

The dynamical model of the converter is adopted using Kirchhoff current and voltage laws:

$$\begin{aligned} \dot{i}_L &= \tfrac{d(t)}{L} v_{dc}(t) - \tfrac{v_b(t)}{L} \\ \dot{v}_{dc} &= \tfrac{D}{C} i_L(t) - \tfrac{i_{load}(t)}{C} \end{aligned} \tag{27}$$

where $d(t)$ is the duty cycle of the switching operation, i_L is the current of the equivalent inductor on the low voltage side of the converter, v_b is the battery voltage and D is the voltage ratio. The converter is controlled using a cascaded PID control approach [38].

2.2.8. State space modeling of energy generation side

In this part, a state space model is presented by combining the components of the energy generation side, i.e., diesel engine, synchronous generator, rectifier, battery, and bidirectional converter. First, (18) is rewritten in matrix form as:

$$\begin{bmatrix} \dot{\psi}_d \\ \dot{\psi}_q \\ \dot{\psi}_{fd} \\ \dot{\psi}_{kd} \\ \dot{\psi}_{kq} \end{bmatrix} = \begin{bmatrix} 0 & \omega_{dg} & 0 & 0 & 0 \\ \omega_{dg} & 0 & 0 & 0 & 0 \\ 0 & 0 & 0 & 0 & 0 \\ 0 & 0 & 0 & 0 & 0 \\ 0 & 0 & 0 & 0 & 0 \end{bmatrix} \begin{bmatrix} \psi_d \\ \psi_q \\ \psi_{fd} \\ \psi_{kd} \\ \psi_{kq} \end{bmatrix} + \begin{bmatrix} r_s & 0 & 0 & 0 & 0 \\ 0 & r_s & 0 & 0 & 0 \\ 0 & 0 & -r_{fd} & 0 & 0 \\ 0 & 0 & 0 & -r_{kd} & 0 \\ 0 & 0 & 0 & 0 & -r_{kq} \end{bmatrix} \begin{bmatrix} i_d \\ i_q \\ i_{fd} \\ i_{kd} \\ i_{kq} \end{bmatrix} + \begin{bmatrix} v_d \\ v_q \\ v_{fd} \\ 0 \\ 0 \end{bmatrix}. \tag{28}$$

Then, by combining the above equation with (20) and (23), we obtain:

$$\begin{aligned} \dot{I}_G &= X_G^{-1} S_\omega(\omega_{dg}) X_G I_G + X_G^{-1} R_G I_G + v_{dc} X_G^{-1} \\ &\begin{bmatrix} \alpha_{rec} \sin(\arctan(\frac{i_d}{i_q}) - \phi_{rec}) \\ \alpha_{rec} \cos(\arctan(\frac{i_d}{i_q}) - \phi_{rec}) \\ 0 \\ 0 \\ 0 \end{bmatrix} + X_G^{-1} b v_{fd} \end{aligned} \tag{29}$$

where I_G is the vector of currents, X_G is the matrix of per unit inductances, and R_G is the diagonal matrix of resistances. Moreover,

$$S_\omega(\omega_{dg}) = \begin{bmatrix} 0 & \omega_{dg} & 0 & 0 & 0 \\ \omega_{dg} & 0 & 0 & 0 & 0 \\ 0 & 0 & 0 & 0 & 0 \\ 0 & 0 & 0 & 0 & 0 \\ 0 & 0 & 0 & 0 & 0 \end{bmatrix}$$

and $b = [0 \;\; 0 \;\; 1 \;\; 0 \;\; 0]^T$.

The dynamics of a diesel-generator shaft speed can now be represented in matrix form as:

$$\begin{aligned} \dot{\omega}_{dg} &= \tfrac{1}{2H}(Q_{en} - I_G X_G^T G_1 I_G) \\ \dot{Q}_{en} &= -\tfrac{Q_{en}}{\tau_s} + K_{en} f_{en}, \end{aligned} \tag{30}$$

where

$$G_1 = \begin{bmatrix} 0 & 1 & 0 & 0 & 0< \\ -1> & 0 & 0 & 0 & 0< \\ 0> & 0 & 0 & 0 & 0< \\ 0> & 0 & 0 & 0 & 0< \\ 0> & 0 & 0 & 0 & 0 \end{bmatrix}.$$

The dynamics of the DC link voltage in the presence of m number of DGR sets can be written as:

$$\dot{v}_{dc} = \frac{1}{C}(\beta_{rec_1} \sqrt{I_{G_1}^T G_2 I_{G_1}} + ...m + \beta_{rec_m} \sqrt{I_{G_m}^T G_2 I_{G_m}} + D i_L - i_{load}) \tag{31}$$

where

$$G_2 = \begin{bmatrix} 1 & 0 & 0 & 0 & 0 \\ 0 & 1 & 0 & 0 & 0 \\ 0 & 0 & 0 & 0 & 0 \\ 0 & 0 & 0 & 0 & 0 \\ 0 & 0 & 0 & 0 & 0 \end{bmatrix}.$$

As a result, the overall dynamics of the energy generation side can be described using the following equations:

$$
\begin{aligned}
&\dot{I}_{G_1} = X_{G_1}^{-1} S_\omega(\omega_{dg_1}) X_{G_1} I_{G_1} + X_{G_1}^{-1} R_{G_1} I_{G_1} \\
&+ v_{dc} X_{G_1}^{-1} E_1 + X_{G_1}^{-1} b v_{fd_1} \\
&\dot{\omega}_{dg_1} = \tfrac{1}{2H_1}(Q_{en_1} - I_{G_1}^T X_{G_1}^T G_1 I_{G_1}) \\
&\dot{Q}_{en_1} = -\tfrac{Q_{en_1}}{\tau_{s_1}} + K_{en_1} f_{en_1} \\
&\vdots \\
&\dot{I}_{G_m} = X_{G_m}^{-1} S_\omega(\omega_{dg_m}) X_{G_m} I_{G_m} + X_{G_m}^{-1} R_{G_m} I_{G_m} \\
&+ v_{dc} X_{G_m}^{-1} E_m + X_{G_m}^{-1} b v_{fd_m} \\
&\dot{\omega}_{dg_m} = \tfrac{1}{2H_m}(Q_{en_m} - I_{G_m}^T X_{G_m}^T G_1 I_{G_m}) \\
&\dot{Q}_{en_m} = -\tfrac{Q_{en_m}}{\tau_{sm}} + K_{en_m} f_{en_m} \\
&\dot{i}_L = \tfrac{d}{L} v_{dc} - \tfrac{v_b(t)}{L} \\
&\dot{v}_{dc} = \tfrac{1}{C}(\beta_{rec_1} \sqrt{I_{G_1}^T G_2 I_{G_1}} + ...m + \beta_{rec_m} \sqrt{I_{G_m}^T G_2 I_{G_m}} + D i_L - i_{load})
\end{aligned} \tag{32}
$$

where

$$
E_j = \begin{bmatrix} \alpha_{rec_j} \sin\left(\arctan\left(\frac{i_{d_j}}{i_{q_j}}\right) - \phi_{rec_j}\right) \\ \alpha_{rec_j} \cos\left(\arctan\left(\frac{i_{d_j}}{i_{q_j}}\right) - \phi_{rec_j}\right) \\ 0 \\ 0 \\ 0 \end{bmatrix}. \tag{33}
$$

For the control of energy generation side and load sharing, conventional PI-based schemes are adopted [17,38].

2.2.9. State space modeling of energy consumption side

Considering (13)–(15) the state space model for an induction motor-propeller set can be written as:

$$
\begin{aligned}
&\dot{I}_M = X_M^{-1} v_M - X_M^{-1} w_M X_M I_M - X_M^{-1} R_M I_M \\
&\dot{\omega}_m = \tfrac{1}{j}(1.5 p_m I_M^T X_M^T M_1 I_M - Q_p)
\end{aligned} \tag{34}
$$

where

$$
w_M = \begin{bmatrix} \omega_p & 0 & 0 & 0 \\ 0 & \omega_p & 0 & 0 \\ 0 & 0 & -(\frac{2}{p_m}\omega_p - \omega_e) & 0 \\ 0 & 0 & 0 & (\frac{2}{p_m}\omega_p - \omega_e) \end{bmatrix}, \tag{35}
$$

$$
R_M = \begin{bmatrix} -r_{sm} & 0 & 0 & 0 \\ 0 & r_{sm} & 0 & 0 \\ 0 & 0 & r_{rm} & 0 \\ 0 & 0 & 0 & r_{rm} \end{bmatrix}, \tag{36}
$$

$$
X_M = \begin{bmatrix} L_{sm} & 0 & L_{mm} & 0 \\ 0 & L_{sm} & 0 & L_{mm} \\ L_{mm} & 0 & L_{rm} & 0 \\ 0 & L_{mm} & 0 & L_{rm} \end{bmatrix}, \tag{37}
$$

$$
M_1 = \begin{bmatrix} 0 & 1 & 0 & 0 \\ -1 & 0 & 0 & 0 \\ 0 & 0 & 0 & 0 \\ 0 & 0 & 0 & 0 \end{bmatrix}, \tag{38}
$$

$I_M = [i_{dsm}, i_{qsm}, i_{rsm}, i_{qrm}]^T$, and $v_M = [v_{dsm}, v_{qsm}, v_{rsm}, v_{qrm}]^T$.

3. Model predictive maneuvering control

MPC approaches enable constraint handling and predicting future values of states and control inputs. These features are advantageous for ship maneuvering control purposes and interaction with the PPS as they can lead to safer and more fuel-efficient ship operations. In this section, an MPC algorithm is proposed for maneuvering control of autonomous ships in 3DoF. The proposed algorithm is based on IOFL where by introduction of an auxiliary control input, a linear relationship is established between the system outputs and auxiliary inputs. Moreover, by adoption of the methodology introduced in [27,28], the constraints are linearized which leads to the possibility of using quadratic programming methods for solving the optimization problem of the MPC algorithm. As a result, the computational costs of the algorithm reduce significantly compared to the algorithms presented in [3,20]. We use the speed dynamics in (1) for the trajectory control. The position dynamics in (1) are used for determining the desired speed of the ship.

Let us rewrite the speed dynamics of the ship as:

$$
\dot{v}_s(t) = M_s^{-1}(\tau_s + \tau_{drag}(v_s(t), \eta_s(t)) - C_s(v_s(t))v_s(t)). \tag{39}
$$

With the following IOFL law the above system can be linearized:

$$
\tau_s = M_s(-\tau_{drag}(v_s(t), \eta_s(t)) + C_s(v_s(t))v_s(t) + A_s v_s + B_s \nu_s) \tag{40}
$$

where ν_s is the input vector of linearized system, ζ_s represents its states and A_s and B_s are states and input matrices of the linear system, respectively. As a result, the transformed linear system can be written as:

$$
\dot{\nu}_s = A_s \nu_s + B_s \nu_s. \tag{41}
$$

After discretization, MPC is applied where the objective is to keep the ship as close as possible to the reference trajectory. In this regard, the following MPC problem is defined with sample time T_k:

$$
\mathbb{P}(\nu_s): \min_{\nu_s} \left(V_N(\nu_s, \nu_s) = \sum_{i=0}^{N-1} l(\nu_s(k+i), \nu_s(k+i)) \right) \tag{42}
$$

subject to:

$$
\begin{aligned}
&\nu_s(k+i+1) = A_s(T_k)\nu_s(k+i) + B_s(T_k)\nu_s(k+i) \\
&\nu_{min}(k+i) \leqslant \nu_s(k+i)(k) \leqslant \nu_{max}(k+i) \\
&\nu_{min}(k+i-1) \leqslant \nu_s(k+i-1) \leqslant \nu_{max}(k+i-1),\ \forall\, i \in [0, N]
\end{aligned} \tag{43}
$$

where

$$
l(\zeta_s(k), \nu_s(k)) = (\zeta_s(k) - \nu_{s_{ref}}(k))^T W_s (\zeta_s(k) - \nu_{s_{ref}}(k)) + \nu_s^T(k)\nu_s(k). \tag{44}
$$

In the above MPC problem, parameter N is the prediction horizon and W_s is the weight matrix of the cost function and is a positive definite matrix.

The reference ship speed $\nu_{s_{ref}}(k)$ is approximated using (1) as:

$$
\nu_{s_{ref}}(k+1) = R^{-1}(\eta_s(k))\left(\frac{\eta_{ref}(k+1) - \eta_s(k)}{T_k}\right). \tag{45}
$$

The adoption of IOFL for MPC results in clear advantages since the optimization problem is simplified, however, due to non-linearity of input constraints, quadratic programming cannot be adopted for solving the optimization problem. In the following, using the results in [28], we adopt a methodology for linearizing the input constraints in (43) to further simplify the optimization problem which leads to major reduction of computational costs.

The main idea behind this methodology is linear estimation of nonlinear constraints. Let us present the constraints acting on the thrust

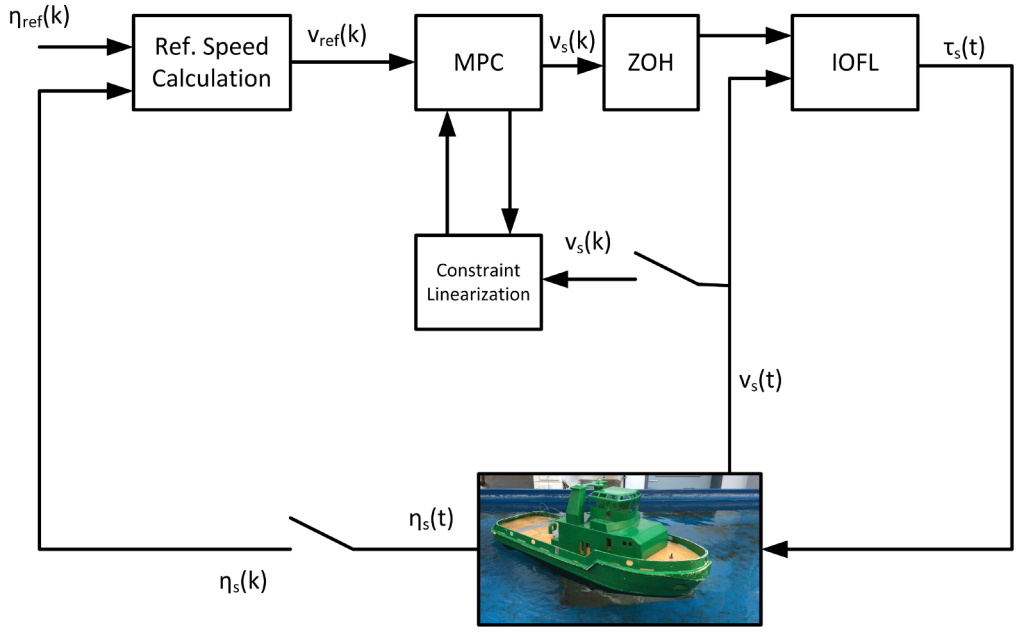

Fig. 4. The block diagram of the proposed maneuvering control strategy.

Fig. 5. Tito-Neri: a harbor tug 1:30 replica model [39].

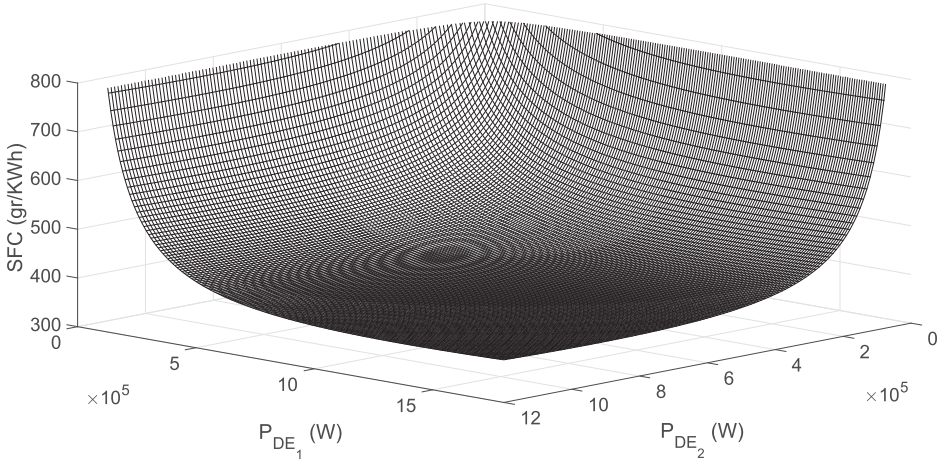

Fig. 6. Combined SFC curve of the harbor tug.

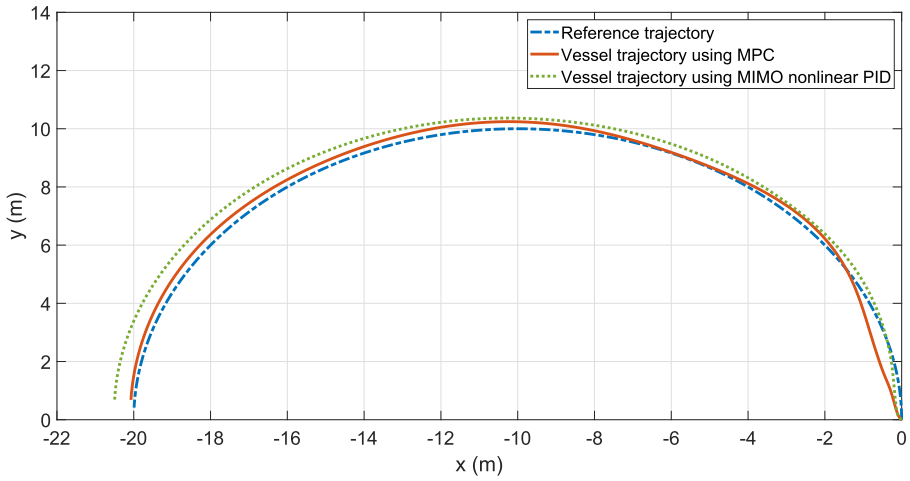

(a) Vessel trajectory compared to the reference trajectory.

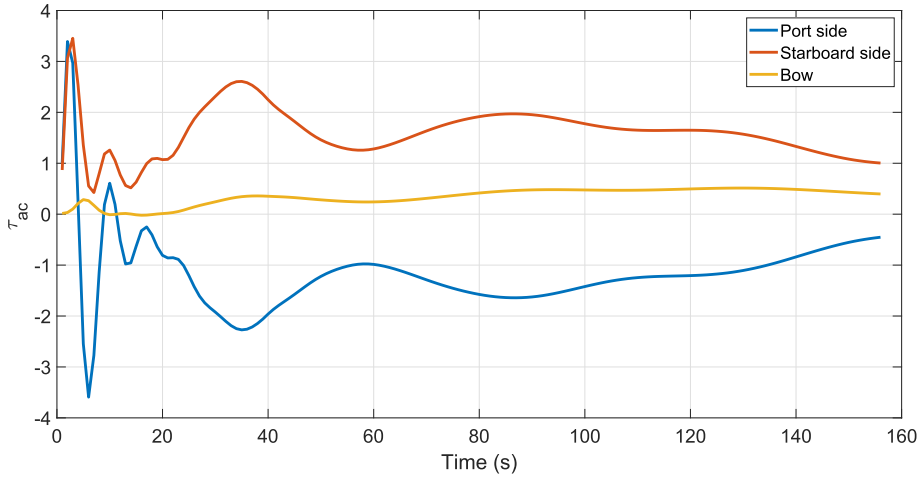

(b) Generated thrust by the actuators (using MPC).

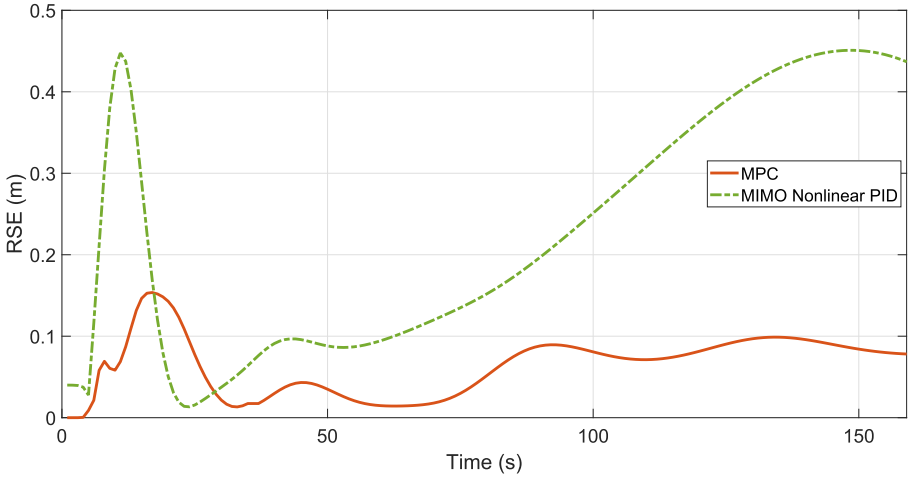

(c) Trajectory tracking error.

Fig. 7. Comparison of th trajectory tracking performance of the ship using the proposed MPC scheme and the conventional PID-based approach.

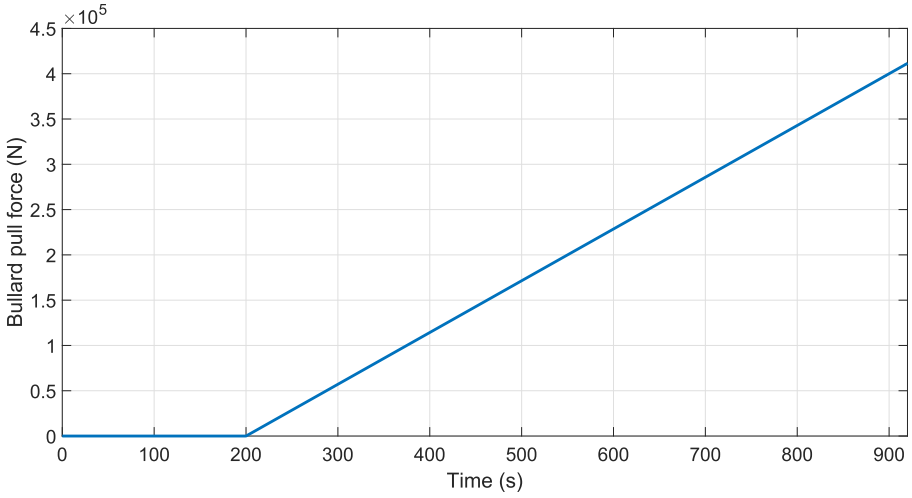

(a) Applied bullard pull force.

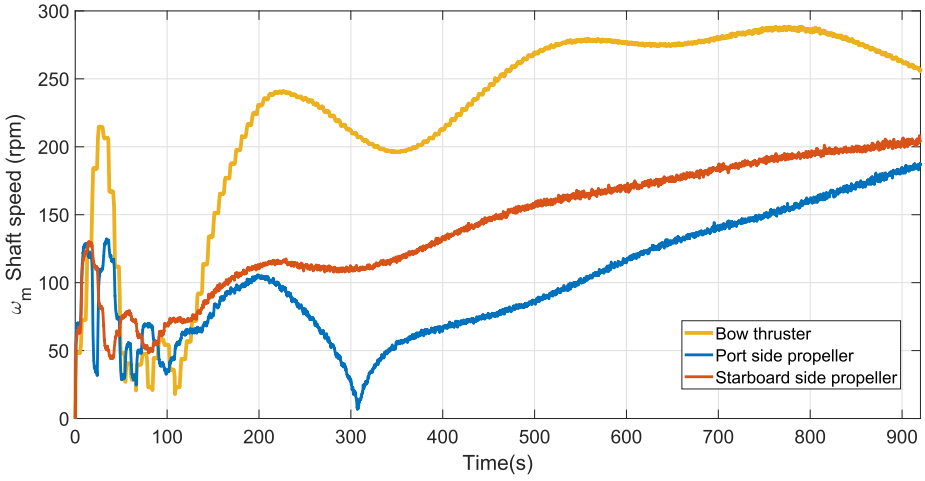

(b) Shaft speed of the propelling actuators.

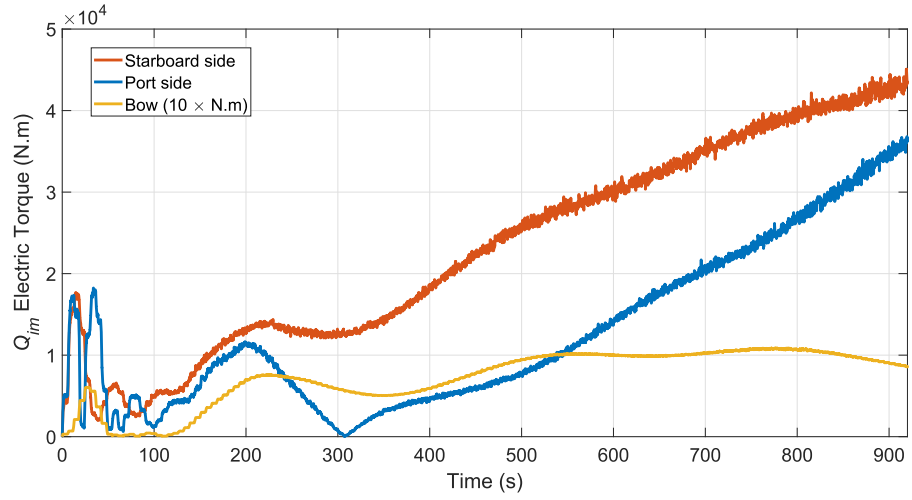

(c) Electric torque of the induction motors.

Fig. 8. Simulation results of the energy consumption side (Experiment I).

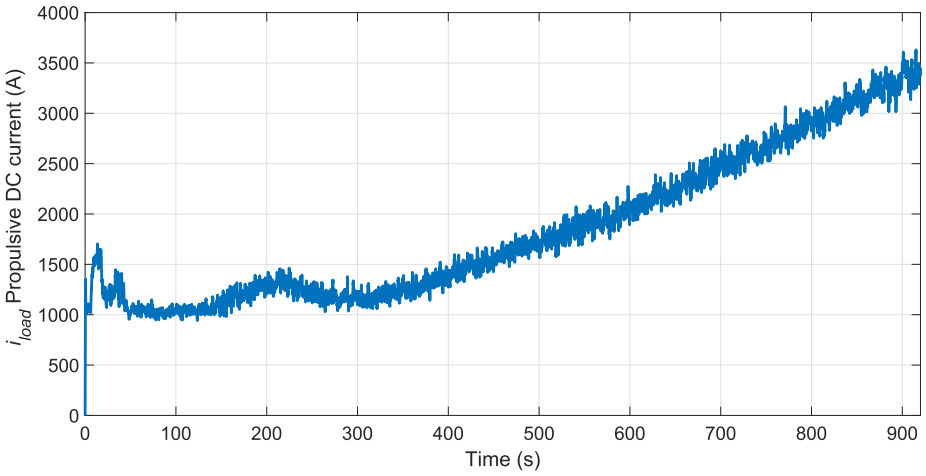

(a) Propulsive load current at DC-link.

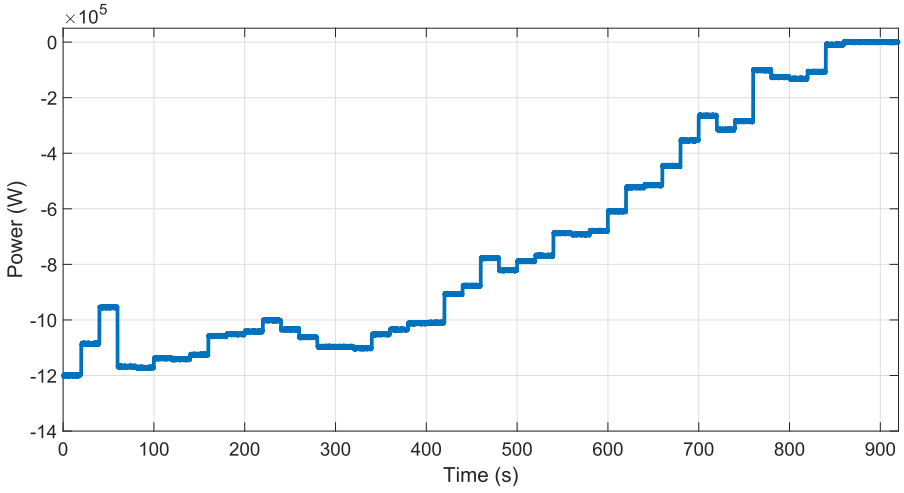

(b) Assigned power for battery charging.

Fig. 9. Load and the battery current in charge mode (Experiment I).

vector τ_s:

$$\tau_{\min} \leqslant \tau_s(k) \leqslant \tau_{\max}. \tag{46}$$

If the IOFL rule is rewritten as:

$$\begin{aligned} \nu_s(t) &= \Psi_s(\nu_s(t), \tau_s(t)) \\ &= B_s^{-1}(M_s^{-1}\tau_s(t) + \tau_{\text{drag}}(\nu_s(t), \eta_s(t)) - C_s(\nu_s(t))\nu_s(t) - A_s\nu_s(t)), \end{aligned} \tag{47}$$

then, ν_s can be approximated around $(\nu_s(t_0), \tau_s(t_0))$ as:

$$\begin{aligned} \nu_s(t) &\approx \hat{\Psi}_{s_{t_0}}(\nu_s(t), \tau_s(t)) \\ &= \Psi_s(\nu_s(t_0), \tau_s(t_0)) + \frac{\partial \Psi_s}{\partial \nu_s}\bigg|_{(\nu_s(t_0),\tau_s(t_0))} (\nu_s(t) - \nu_s(t_0)) + \frac{\partial \Psi_s}{\partial \tau_s}\bigg|_{(\nu_s(t_0),\tau_s(t_0))} \\ &\quad (\tau_s(t) - \tau_s(t_0)). \end{aligned} \tag{48}$$

Let $\nu_s(k+i|k)$ denotes the value of ν_s at time $(k+i)t_k$ predicted at time kt_k, then using (48), the linear constraints can be found as:

$$\begin{aligned} \nu_{\min}(k+i-1) &= \min_{\tau_s(k+i-1)} \hat{\Psi}_{s_{k+i|k-1}}(\nu_s(k+i|k-1), \tau_s(k+i-1)) \\ \nu_{\max}(k+i-1) &= \max_{\nu_2(k+i-1)} \hat{\Psi}_{s_{k+i|k-1}}(\nu_s(k+i|k-1), \tau_s(k+i-1)) \end{aligned} \tag{49}$$

subject to,

$$\tau_{\min} \leqslant \tau_s(k+i-1) \leqslant \tau_{\max}, \quad \forall\, i \in [0, N-1]. \tag{50}$$

Note that for time instant $(k+N-1)t_k$, we have:

$$\begin{aligned} \nu_{\min}(k+N-1) &= \nu_{\min}(k+N-2) \\ \nu_{\max}(k+N-1) &= \nu_{\max}(k+N-2). \end{aligned} \tag{51}$$

Note also that, due to the linearity of $\hat{\Psi}_{s_{k+i|k-1}}(.)$, the optimization problems in (49) are trivial to solve.

The adoption of this methodology leads to simplification of the optimization problem within MPC and to the possibility of using a quadratic programming scheme. The block diagram of the proposed control approach is depicted in Fig. 4.

At every sample time k, the proposed control algorithm generates a set of control inputs $\nu_s(k|k)$, …, $\nu_s(k+N-1|k)$ and $\nu_s(k|k)$, …, $\nu_s(k+N-1|k)$. Using these sets and (40), the set of future control inputs $\tau_s(k|k)$, …, $\tau_s(k+N-1|k)$ can be estimated. By adoption of (12) and (13), the set of future power demand for propelling the ship over horizon N can be approximated that is $P_s(k|k)$, …, $P_s(k+N-1|k)$. In the next section, we propose an energy management strategy that will utilize this set.

4. Predictive energy management

In this section, an energy management algorithm is proposed for the purpose of finding the optimal split between the different energy sources, namely, the DGR sets and the battery-converter set. The

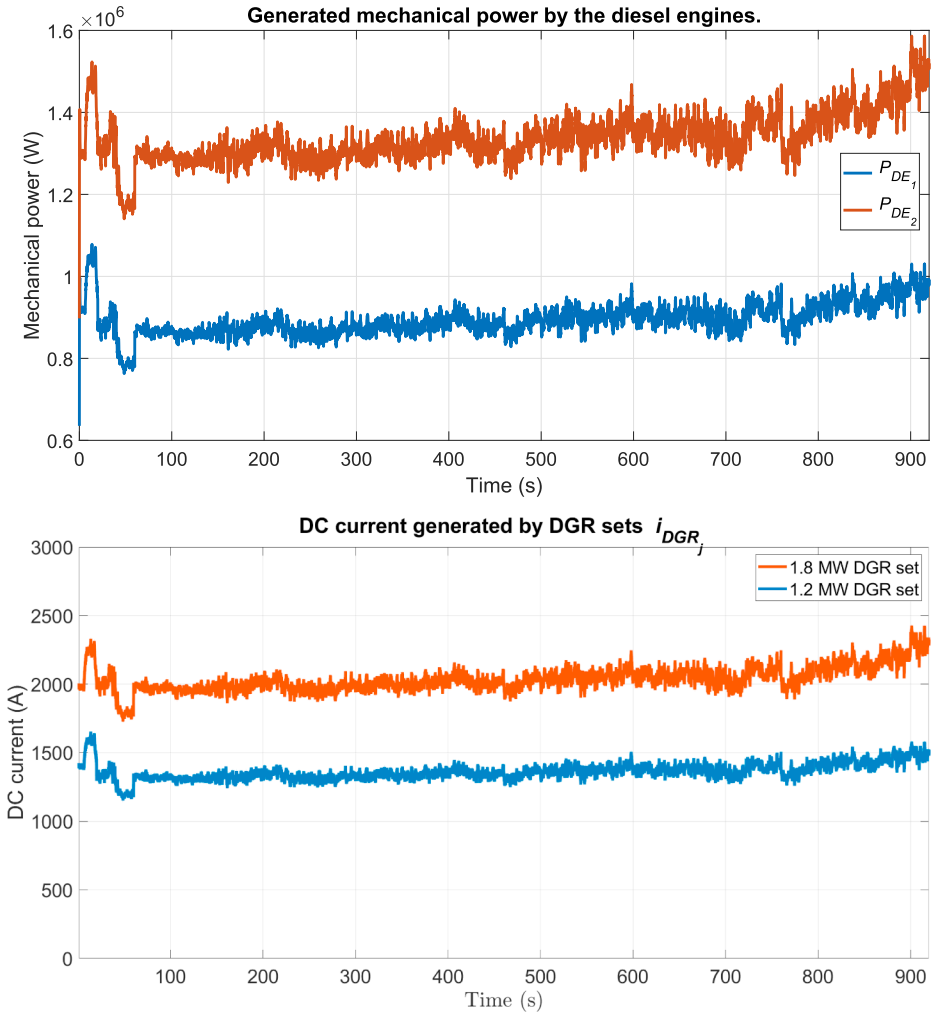

Fig. 10. Generated power and current by the energy sources (Experiment I).

objective is to keep the diesel-generators functioning around their optimal point in the Specific Fuel Consumption (SFC) curve which leads to an efficient performance. Furthermore, the algorithm limits DGR sets to experience sudden changes in loading condition which results in higher robustness of the DC-PPS.

In the following, the cost function of the PEM problem that is based on the SFC curve of diesel engines is derived. SFC curve is an indicator for fuel-efficient power and energy generation. The SFC curve of a diesel engine can be represented as:

$$SFC\,(P_{\mathrm{DE}}) = \frac{a}{P_{\mathrm{DE}}} + bP_{\mathrm{DE}} + c \tag{52}$$

where P_{DE} is the delivered mechanical power and a, b and c are parameters dependent on the diesel engine specifications.

The electrical losses in energy generation side of the power network are functions of the output power of the diesel engine [31]. In this paper, based on the results in [17], the copper, iron, mechanical and rectifier losses of the generator-rectifier set are included in the problem by a constant coefficient, i.e., $P_{\mathrm{DGR}} = \alpha_{\mathrm{DGR}} P_{\mathrm{DE}}$ where $0 < \alpha_{\mathrm{DGR}} < 1$ which depends on the specifications of the generator-rectifier set. The same approach is also considered for the set of battery-converter. As a result, $P_{\mathrm{BC}} = \alpha_{\mathrm{BC}} P_{\mathrm{B}}$ where $0 < \alpha_{\mathrm{BC}} < 1$. Since, the efficient region in the SFC curve is a wide area, this approximation does not affect the optimality of the process, significantly.

The power share assigned at time kt_{k} that should be delivered by DGR set j over horizon N_{E} is denoted as $P_{\mathrm{DGR}_j}(k|k)$, $P_{\mathrm{DGR}_j}(k+1|k)$, ...,$P_{\mathrm{DG}_j}(k+i-1|k)$. Similarly, the assigned power to be delivered by the battery-converter set is $P_{\mathrm{BC}}(k|k)$, $P_{\mathrm{BC}}(k+1|k)$, ...,$P_{\mathrm{BC}}(k+i-1|k)$ over the horizon N_{E}. Considering these sets, the following relationships are consistent:

$$\begin{aligned} P_{\mathrm{DG}_i}(k+i-1|k) &= v_{\mathrm{DC}}\, i_{\mathrm{DG}_j}(k+i-1|k) \\ P_{\mathrm{BC}}(k+i-1|k) &= v_{\mathrm{DC}}\, i_{\mathrm{BC}}(k+i-1|k), \end{aligned} \tag{53}$$

where v_{DC} is the DC voltage of the power network, which must be kept constant around a certain value and $i_{\mathrm{DG}i}$, and $i_{\mathrm{BC}i}$ are current shares provided by DGR i and battery-converter sets, respectively.

The efficient delivered power by diesel engine i is denoted as P_{eff_i} and defined as:

$$P_{\mathrm{eff}_i} = \underset{P_{\mathrm{m}i}}{\mathrm{Arg\,min}}\ (SFC\,(P_{\mathrm{m}i})). \tag{54}$$

As a result, the first goal of the algorithm is to keep $\frac{P_{\mathrm{DGR}_j}(k+i-1\,|\,k)}{\alpha_{\mathrm{DGR}}}$ around P_{eff_j}.

It is assumed that the different sets of diesel-generators can have different specifications with different P_{eff_i} and maximum power that they can deliver. Since the power demand changes over the operation time, first the set of active DGRs should be determined using specifications of DGRs (i.e., P_{eff_i} and their power ratings) as well as the power demand $P_{\mathrm{d}}(k)$. For this goal, a set of optimization problems needs to be solved over the prediction horizon. The optimization problems for charge and discharge modes are different. For the battery discharge mode, we have:

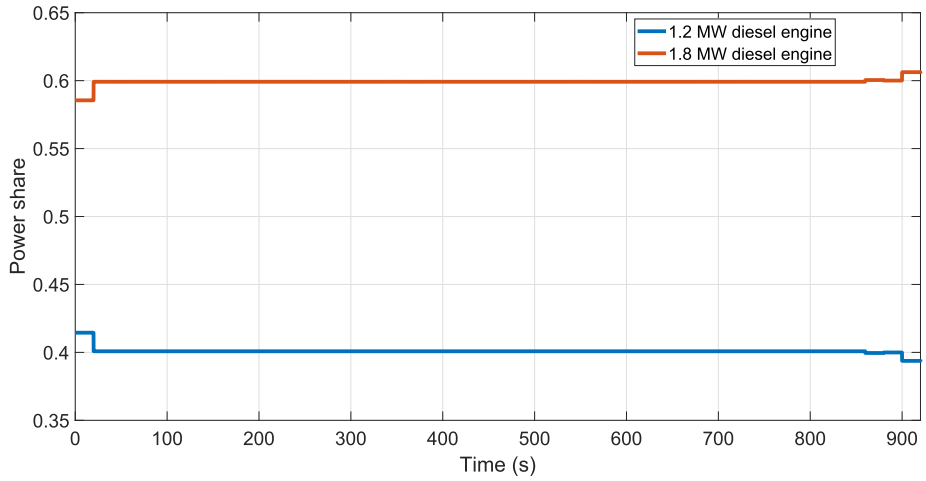

(a) Power share of the DGR sets.

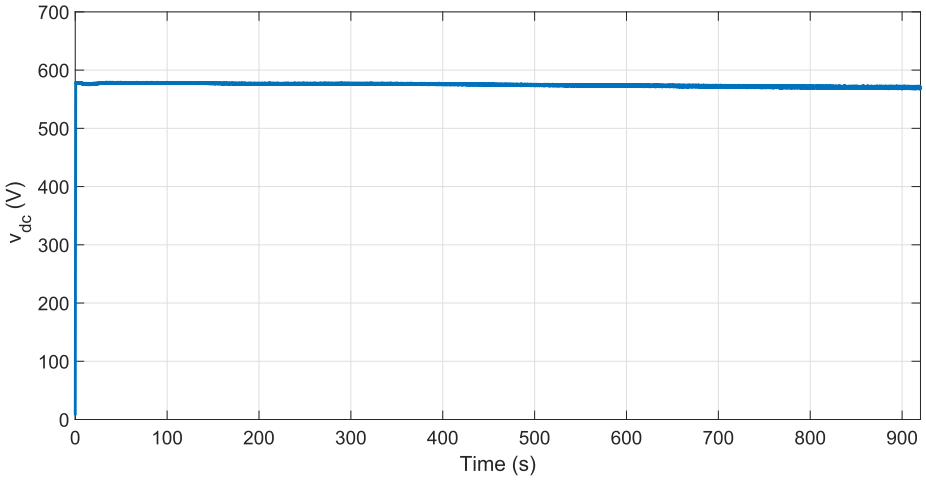

(b) Voltage of the DC-link capacitor.

Fig. 11. Stability results of the power system. (Experiment I).

$$\mathcal{P}^{l}_{\mathrm{DGR}_d}: \min_{\phi_i^l} J_{\mathrm{DGR}_l}(\phi_1^l, \ldots, \phi_m^l) \tag{55}$$

subject to

$$\frac{\phi_1^l}{\alpha_{\mathrm{DGR}_1}} P_{\mathrm{eff}_1} + \ldots + \frac{\phi_m^l}{\alpha_{\mathrm{DGR}_m}} P_{\mathrm{eff}_m} + P_{\mathrm{BC}}(l|k) \geqslant P_{\mathrm{d}}(l|k) \quad \forall\, l \in [k, k+i-1], \quad \forall\, i \in [0, N] \tag{56}$$

The optimization problems in battery charge mode are:

$$\mathcal{P}^{l}_{\mathrm{DGR}_c}: \min_{\phi_i^l} J_{\mathrm{DGR}_l}(\phi_1^l, \ldots, \phi_m^l) \tag{57}$$

subject to

$$\frac{\phi_1^l}{\alpha_{\mathrm{DGR}_1}} P_{\mathrm{eff}_1} + \ldots + \frac{\phi_m^l}{\alpha_{\mathrm{DGR}_m}} P_{\mathrm{eff}_m} \geqslant P_{\mathrm{d}}(l|k)\ \forall\, l \in [k, k+i-1], \quad \forall\, i \in [0, N] \tag{58}$$

Note that for the charge mode, P_{BC} is included in P_{d}. Function J_{DGR_l} is defined as:

$$J_{\mathrm{DGR}_l}(P_{\mathrm{eff}_1}, \ldots, P_{\mathrm{eff}_m}) = \phi_1^l SFC_1(P_{\mathrm{eff}_1}) + \cdots + \phi_m^l SFC_m(P_{\mathrm{eff}_m}), \tag{59}$$

where m is the overall number of DGR sets and $\phi_1, \phi_2, \ldots, \phi_m$ are binary numbers with 0 or 1 values. If $\phi_j^l = 1$ then DGR set j is considered active during the sample time period t_{k}. Since the number of DRG sets onboard of a ship is limited, the above optimization problems are trivial. Note that for the charge mode, P_{BC} is negative.

For constructing the main objective function in this part, we define the following function using (52):

$$S_{\mathrm{j}}(i_{\mathrm{DG}_j}(k+i-1|k)) = \frac{\alpha_{\mathrm{DGR}_j} a_{\mathrm{j}}}{v_{\mathrm{DC}} i_{\mathrm{DGR}_j}(k+i-1|k)} + \frac{b_{\mathrm{j}}}{\alpha_{\mathrm{DGR}_j}} v_{\mathrm{DC}} i_{\mathrm{DGR}_j}(k+i-1|k) \tag{60}$$

where a_{j} and b_{j} are SFC coefficients of diesel engine j defined in (52). Suppose $\mathbb{I}_{\mathrm{DGR}}$ is the set of $i_{\mathrm{DGR}_j}(k+i-1|k)$ for all $j \in [1, m]$ and $i \in [0, N]$, then by employing (60), the cost function for the PEM problem can be formulated as:

$$J_{\mathrm{pm}}(\mathbb{I}_{\mathrm{DGR}}) = \sum_{i=0}^{N} \sum_{j=1}^{m} \phi_i^j S_{\mathrm{i}}(i_{\mathrm{DGR}_j}(k+i-1|k)). \tag{61}$$

The inequality constraints are divided into two types. The first type of constraints are used to keep the energy sources operating in a safe predefined zones. The second type of constraints are employed to prohibit occurrence of major changes in loading condition of energy sources in short intervals to prevent instability in the DC power network. Take var(.) as the variance operator, then the inequality constraints are as below:

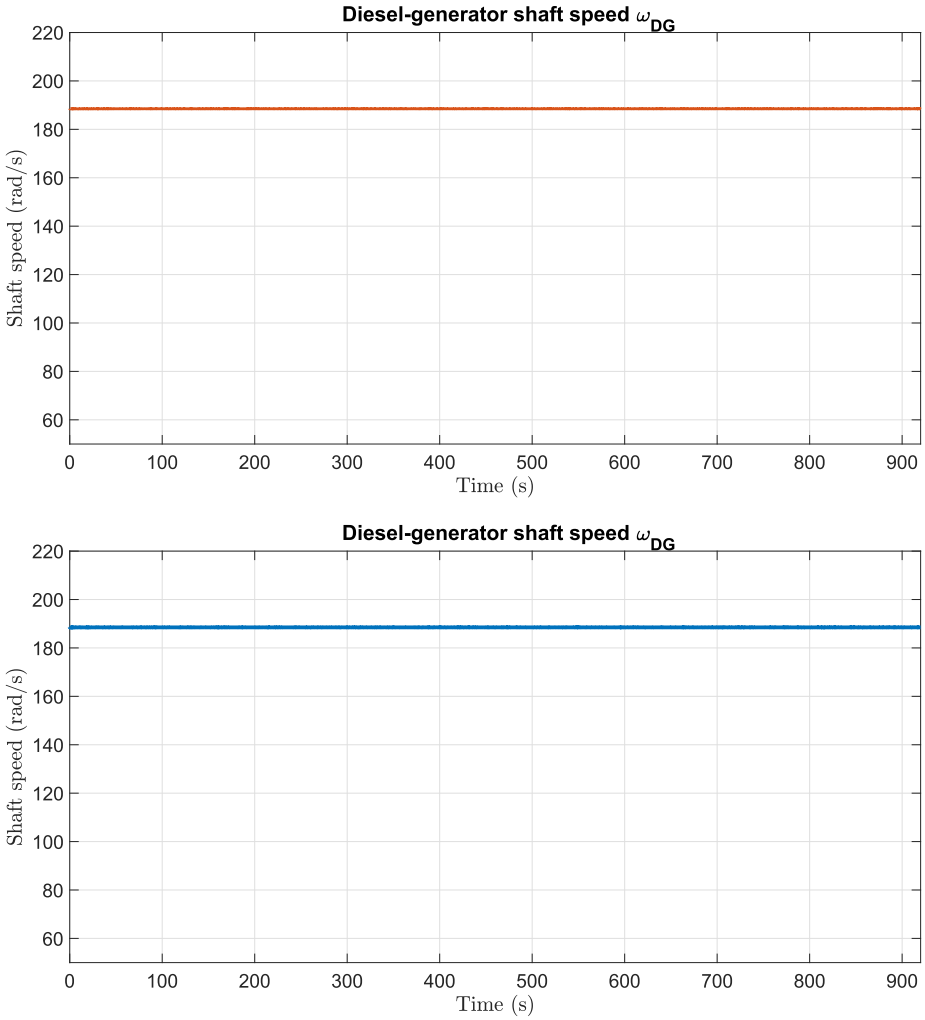

Fig. 12. Diesel-generators shaft speeds. Top: 1.8 MW diesel-generator, bottom: 1.2 MW diesel-genrator (Experiment I).

$$\begin{aligned}
&\text{var}(\phi_1^k i_{\text{DGR}_1}(k|k),...,\phi_1^{(k+N-1)} i_{\text{DGR}_1}(k+N-1|k)) \leqslant M_1\\
&\vdots\\
&\text{var}(\phi_m^k i_{\text{DGR}_m}(k|k),...,\phi_m^{(k+N-1)} i_{\text{DGR}_m}(k+N-1|k)) \leqslant M_m\\
&i_{\text{DGR}_1}(k|k),...,i_{\text{DGR}_1}(k+N-1|k) \leqslant i_{M_1}\\
&\vdots\\
&i_{\text{DGR}_m}(k|k),...,i_{\text{DGR}_m}(k+N-1|k) \leqslant i_{M_m}.
\end{aligned} \tag{62}$$

The battery constraints depend on its operation mode, i.e., charge or discharge. During discharge the following constrains must be handled.

$$\begin{aligned}
&\text{var}(i_{\text{BC}}(k|k),...,i_{\text{BC}}(k+N-1|k)) \leqslant M_{BC}^d\\
&i_{\text{BC}}(k|k),...,i_{\text{BC}_m}(k+N-1|k) \leqslant i_{M_{BC}}^d
\end{aligned}. \tag{63}$$

Similarly for the charge mode, the constrains are as follows:

$$\begin{aligned}
&\text{var}(i_{\text{BC}}(k|k),...,i_{\text{BC}}(k+N-1|k)) \leqslant M_{BC}^c\\
&i_{\text{BC}}(k|k),...,i_{\text{BC}_m}(k+N-1|k) \geqslant i_{M_{BC}}^c
\end{aligned} \tag{64}$$

where M_{BC}^d, M_{BC}^c and $i_{M_{BC}}^d$ are positive and $i_{M_{BC}}^c$ is negative.

The equality constrains are established to keep the sum of power shares equal to the demanded power:

$$\begin{aligned}
&\phi_1^k P_{\text{DGR}_1}(k|k)+...+\phi_m^k P_{\text{DGR}_m}(k|k) + P_{\text{BC}}(k|k) = P_{\text{d}}(k|k)\\
&\vdots\\
&\phi_1^{(k+N-1)} P_{\text{DGR}_1}(k+N-1|k)+...+\phi_m^{(k+N-1)} P_{\text{DGR}_m}(k+N-1|k)\\
&+ P_{\text{BC}}(k+N-1|k) = P_{\text{d}}(k+N-1|k)
\end{aligned} \tag{65}$$

where $P_{\text{DGR}_j}(.)$ and $P_{\text{BC}}(.)$ are calculated using (53). Now, the optimization problem can be formulated as:

$$\mathcal{P}_{\text{pm}}: \min_{\mathbb{I}_{\text{DGR}}} J(\mathbb{I}_{\text{DG}}) \tag{66}$$

subject to constraints in (62)–(65).

Remark 1. The cost function in (61) is a sum of multiple convex functions. As a result, it is convex and convex optimization methods can be used for solving the optimization problem in (66).

Remark 2. The presented PEM algorithm can guarantee maximum efficiency for any set of DGRs accompanied by a BC set with different power ratings and SFC curves if the maximum charge/discharge power by the battery at the desired voltage v_{dc} is greater or equal to P_{eff} of the diesel engine with the highest power rating, i.e.,

$$\max\{i_{M_{BC}}^d, |i_{M_{BC}}^c|\} \geqslant \max\{\frac{P_{\text{eff}_1}}{\alpha_{\text{DGR}_1} v_{\text{dc}}}, ..., \frac{P_{\text{eff}_m}}{\alpha_{\text{DGR}_m} v_{\text{dc}}}\}. \tag{67}$$

If the above non-equality does not hold, then, finding the optimal split between energy sources using SFC curves is not guaranteed for all time instants kt_{k}.

The above remark indicates that during the design stage, the on-board energy sources should be chosen with regard to achieving optimal fuel efficiency. If this is not the case and (67) does not hold, then, achieving optimal fuel efficiency is not guaranteed.

Remark 3. Using the presented algorithm and based on the predicted power demand over horizon N, the safe turn on/turn off time of DGR

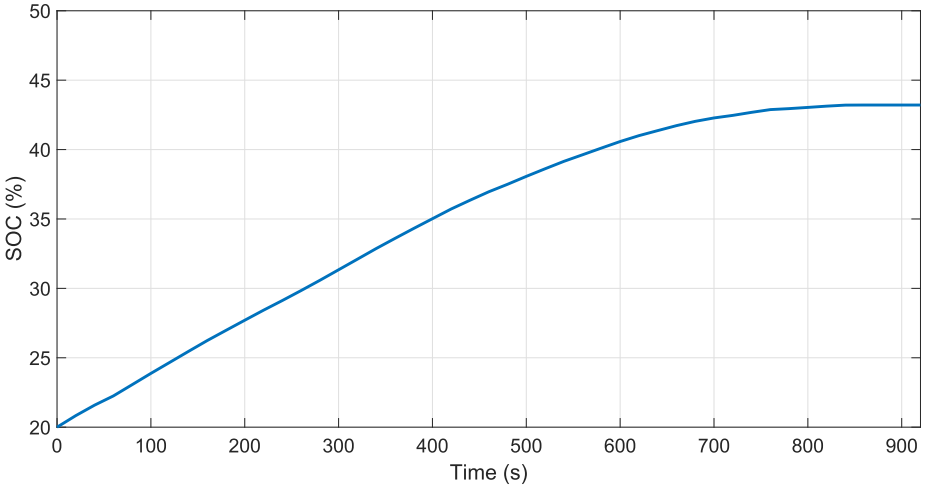

(a) Battery SOC during the voyage.

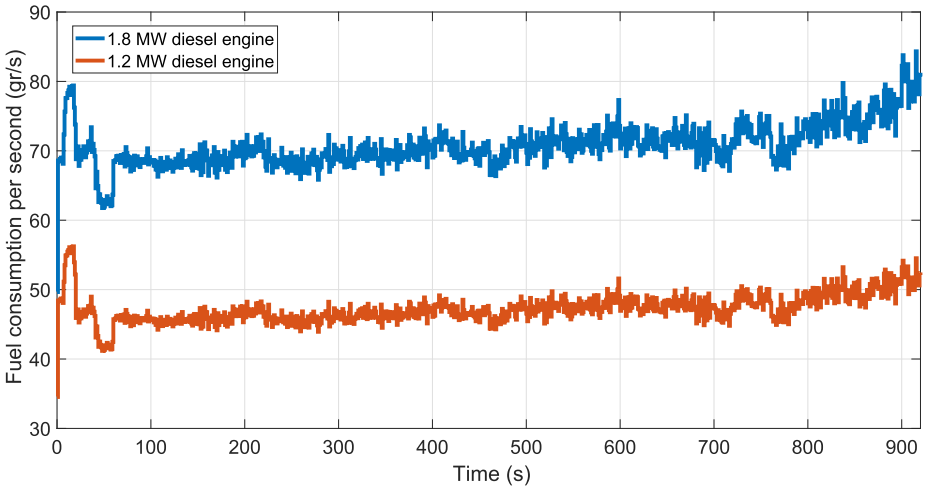

(b) Fuel consumption rate of diesel engines.

Fig. 13. Battery SOC and the fuel consumption rate (Experiment I).

sets can be predicted. Since, it takes some time (warm up time) for DGR sets to be able to provide power for the power network, this prediction can lead to increased safety and robustness in the system. However, modeling the warm-up dynamics of the DGR sets are out of the scope of this paper and are not considered in the simulation cases.

Remark 4. The uncertainties, which are the result of environmental disturbances as well as modeling mismatches, can lead to inaccurate prediction of the future required propulsive power. Since using the proposed energy management approach no diesel engine is fully loaded, in the case of uncertainties within the prediction of the future required power, a great amount of the power capacity is always available to compensate sudden overshoots or increases in the propulsive load.

5. Model predictive maneuvering and energy management control

In this section, the interaction between maneuvering controller and energy management controller is presented explicitly. It is shown how the data from the maneuvering controller can be used by the energy management controller, so that the power availability is guaranteed during the operation.

The following algorithms represent the overall predictive approach for the ship control. The maneuvering control algorithm steps are:

- **Initialization:** Let $\eta_s(0) = \eta_0$, $v_s(0) = v_0$.
  1. Compute $v_{\text{ref}}(k+i) = \frac{\eta_{\text{ref}}(k+i) - \eta_0}{iT_s}$, for all $i = 0, \ldots, N-1$ where T_s is the sample time of predictive maneuvering controller.
  2. Solve the optimization problem in (42) using the constraint linearization approach in (49).
  3. Gather the predicted required thrust over the horizon $\tau_s(k), \ldots, \tau_s(k+N-1)$, solve the thrust allocation problem in (11) to determine the desired speed of propellers.
  4. Using the model of propellers in (12) and (13) and the efficiency curve of inductions motors estimate the future power demand P_d over the horizon N.
  5. Send P_d to the energy management controller and desired speed of actuators to induction motor controllers. Go to 1.

The energy management controller steps are:

- **Initialization:** Determine the initial charge or discharge mode, $P_d(0)$, and obtain the set of active DGR sets.
  1. Depending on the discharge or charge mode of the battery solve the optimization problem in (55) or (57) to select the active DGR sets.

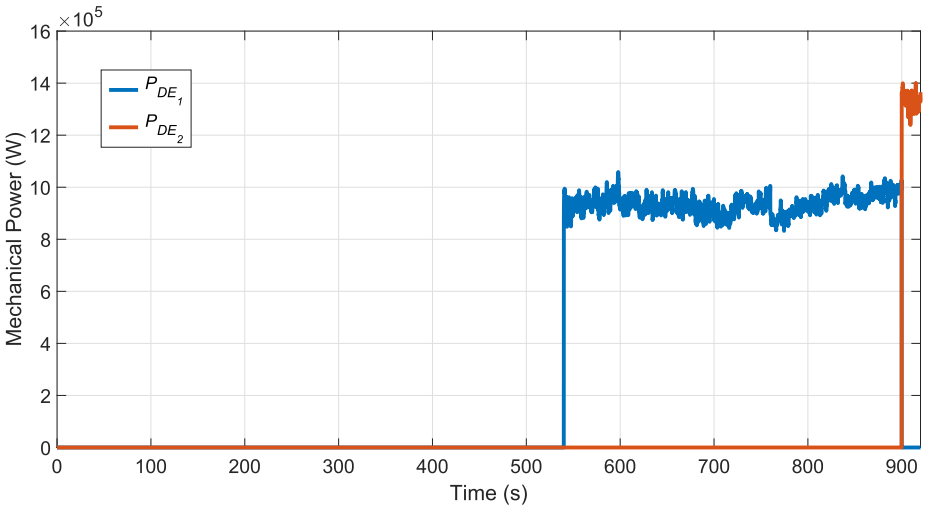

(a) Delivered power by the diesel engines.

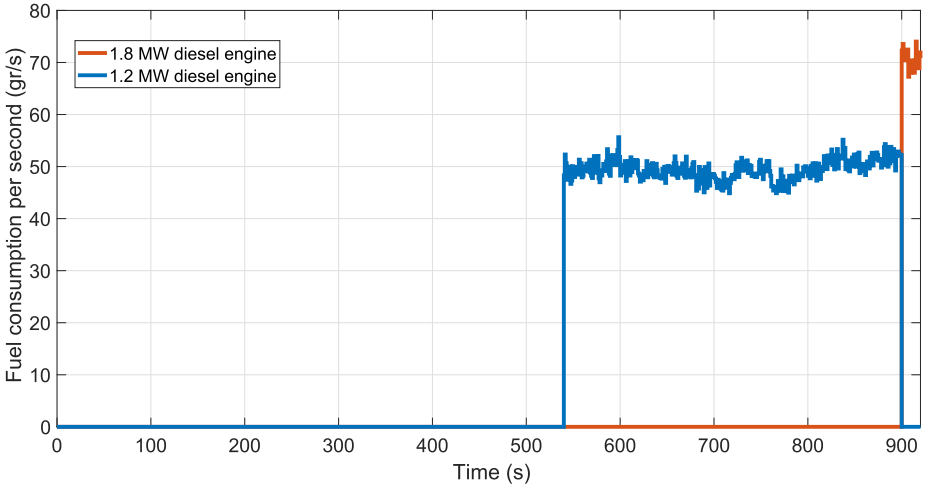

(b) Fuel consumption rate.

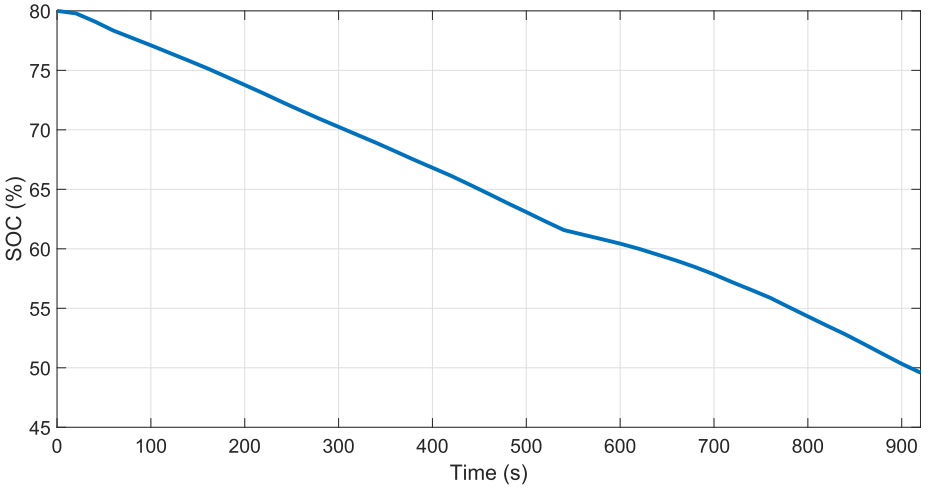

(c) Battery SOC.

Fig. 14. Simulation results in battery discharge mode using PEM (Experiment I).

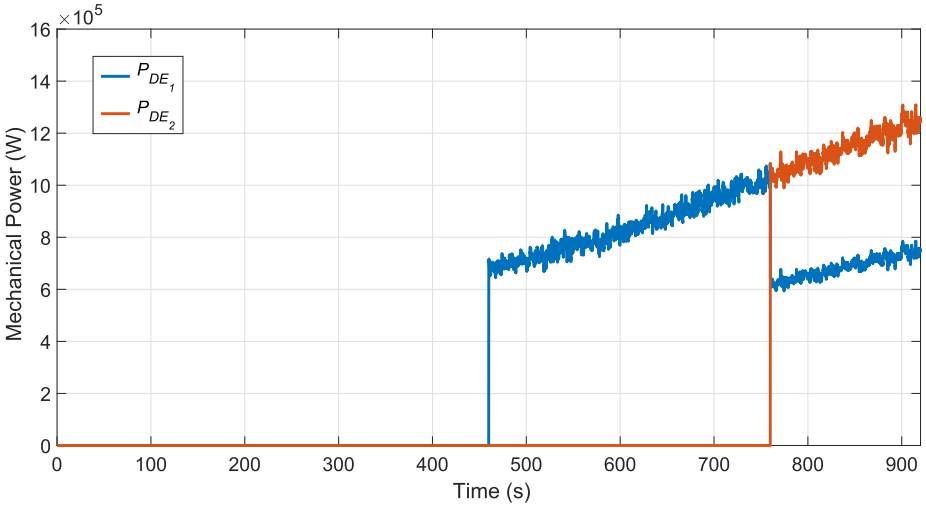

(a) Diesel engine power.

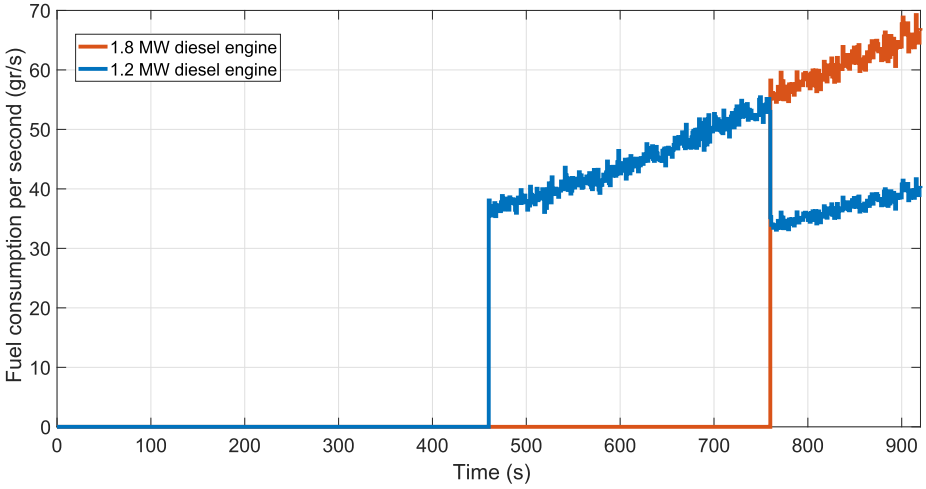

(b) Fuel consumption rate.

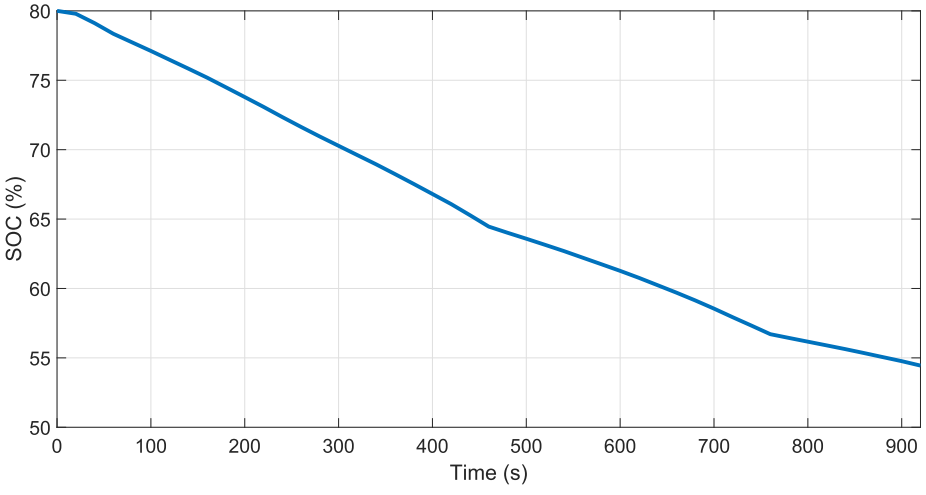

(c) Battery SOC.

Fig. 15. Simulation results using the rule-based approach in discharge mode (Experiment I).

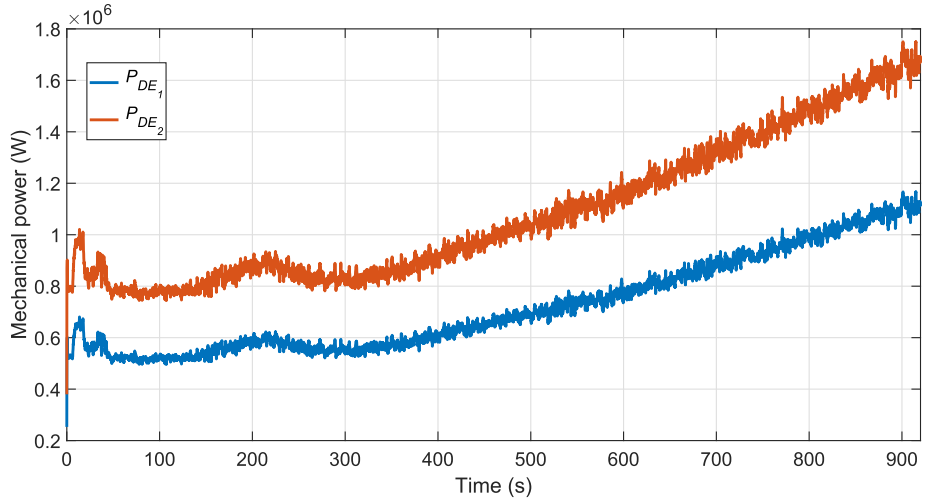

(a) Diesel engine power.

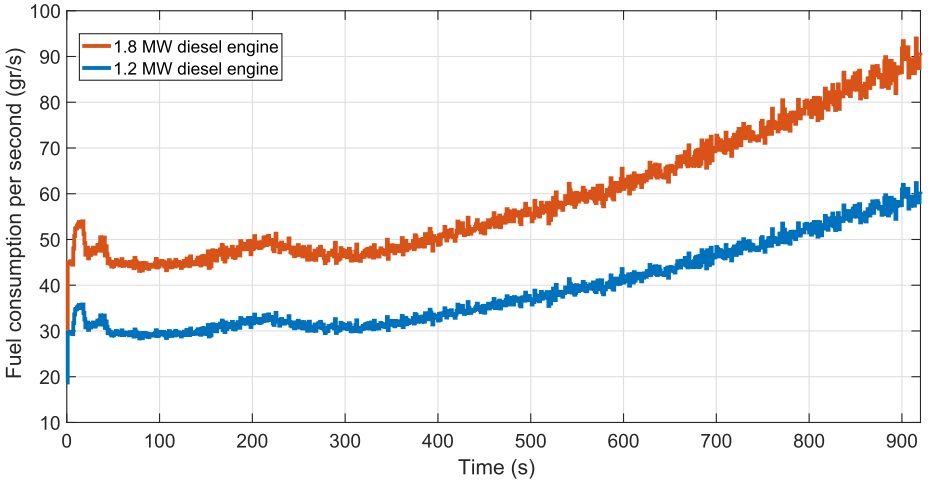

(b) Fuel consumption rate.

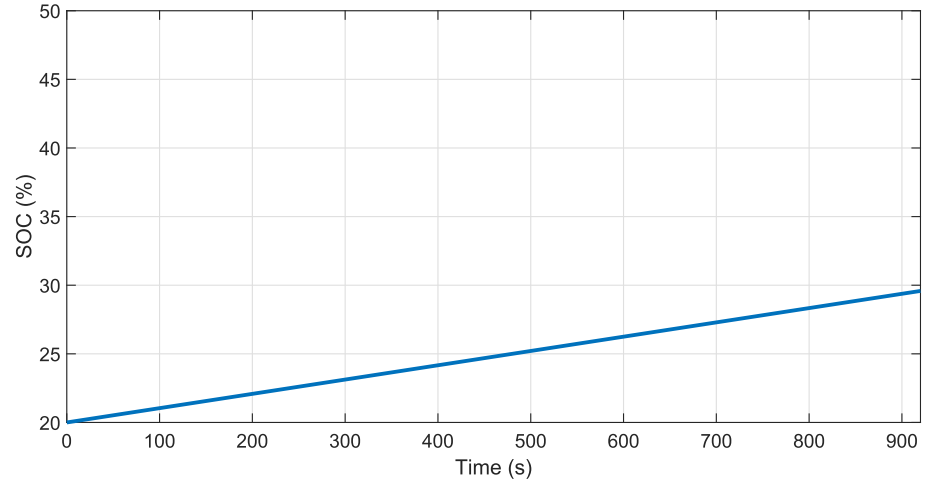

(c) Battery SOC.

Fig. 16. Simulation results using the rule-based approach in charge mode (Experiment I).

Table 1
Overall fuel consumption and generated energy (Experiment I).

Battery mode	Algorithm	Fuel cons. (kg)	Mech. energy (kWh)	SFC	SOC change (%)
Charge	PEM	108.6	567	190.5	23.2
Charge	RB	90	461	195.2	7.2
Discharge	PEM	19.2	101	188.1	−30.4
Discharge	RB	29.1	151.6	192.1	−25.5

2. Solve the optimization problem in (66).
3. Obtain the set of active DGR sets, receive P_d from the maneuvering controller, and go to 1.

Remark 5. Step 1 in the energy management algorithm can be revisited less compared to other steps to avoid activation/deactivation of DGR sets in short time periods. Although this might lead to sub-optimality but it can increase the stability of the network and decreases the maintenance costs and efforts.

Remark 6. If the prediction horizon of the energy management problem N_E is greater than the horizon of the ship maneuvering control problem N, $P_d(k+N)$ can be extended over the remainder of N_E.

In the next section, several simulation results are provided for evaluating the performance of the proposed approach.

6. Simulation-based evaluation

In this section, several experimental results are presented for evaluation of the presented predictive ship control and energy management approach. For the trajectory tracking control, a model vessel known as *Tito-Neri* (Fig. 5) is chosen which represents a 1:30 replica model of a harbor tug [39]. For energy management purposes, the torque and thrust of the model vessel are scaled up using Froude scaling to cope with the real size vessel's PPS. The Tito-Neri maneuvering model is provided in Appendix A.

For the real size harbor tug a 4.4 MW DC-PPS is considered. On the energy generation side, two diesel engines with 1.8 MW and 1.2 MW maximum deliverable power are considered which are accompanied by a battery-converter set which can deliver up to 1.4 MW of power. On the energy consumption side, two 1.5 MW induction motors for propellers and a 500 kW induction motor for actuating the bow thruster are considered. A schematic view of the DC-PPS is provided in Fig. 2. The specification of the system components are provided in the appendix. For the simulations, MATLAB® 2018a is used. For solving the optimization problem of the predictive maneuvering control approach a quadratic programming approach is used and for solving the PEM's optimization problem an interior-point method is adopted.

The combined SFC curve of the overall DC-PPS is provided in Fig. 6, indicating the fuel efficiency of the overall system. The generated and the demanded power construct the following equality constraint at any time instant k:

$$\alpha_{DGR_1} P_{DE_1}(k) + \alpha_{DGR_2} P_{DE_2}(k) + P_{BC}(k) = P_d(k), \tag{68}$$

which represents a surface plane if it is included in Fig. 6. One of the objectives of the proposed PEM algorithm is to guarantee that this surface plane includes the optimal point in the combined SFC curve of Fig. 6 or passes it at a very short distance, depending on the operating and loading conditions.

In this section, results of three different experiments are presented. In the first experiment, a circular trajectory is considered in which the vessel increases its speed. In the second experiment, the trajectory of a real vessel that is based on Automatic Identification System (AIS) data obtained from the port of Rotterdam Authority is simulated. In the final part, the performance of the proposed PEM algorithm is experimented with different operating profiles.

6.1. Experiment I: Circular trajectory

The specifications of the considered trajectory is:

$$\eta_{ref}(t) = \begin{bmatrix} \eta_{ref_x}(t) \\ \eta_{ref_y}(t) \\ atan2(\dot{\eta}_{ref_x}, \dot{\eta}_{ref_y}) \end{bmatrix} \tag{69}$$

$$\eta_{ref_x}(t) = \gamma \cos(\frac{\beta t}{\gamma}), \quad \eta_{d_y}(t) = \gamma \sin(\frac{\beta t}{\gamma}) \tag{70}$$

where γ and β are the radius of the circular trajectory and traveling speed, respectively. It is assumed that $V(0) = [0,\ 0,\ 0]^T$, $\eta_s(0) = [0,\ 0,\ 0]^T$, $\gamma = 10$ and $\beta = 0.2$ m/s. Note that in this experiment the reference speed is constant. It is assumed

Fig. 17. The ship trajectory in the port of Rotterdam.

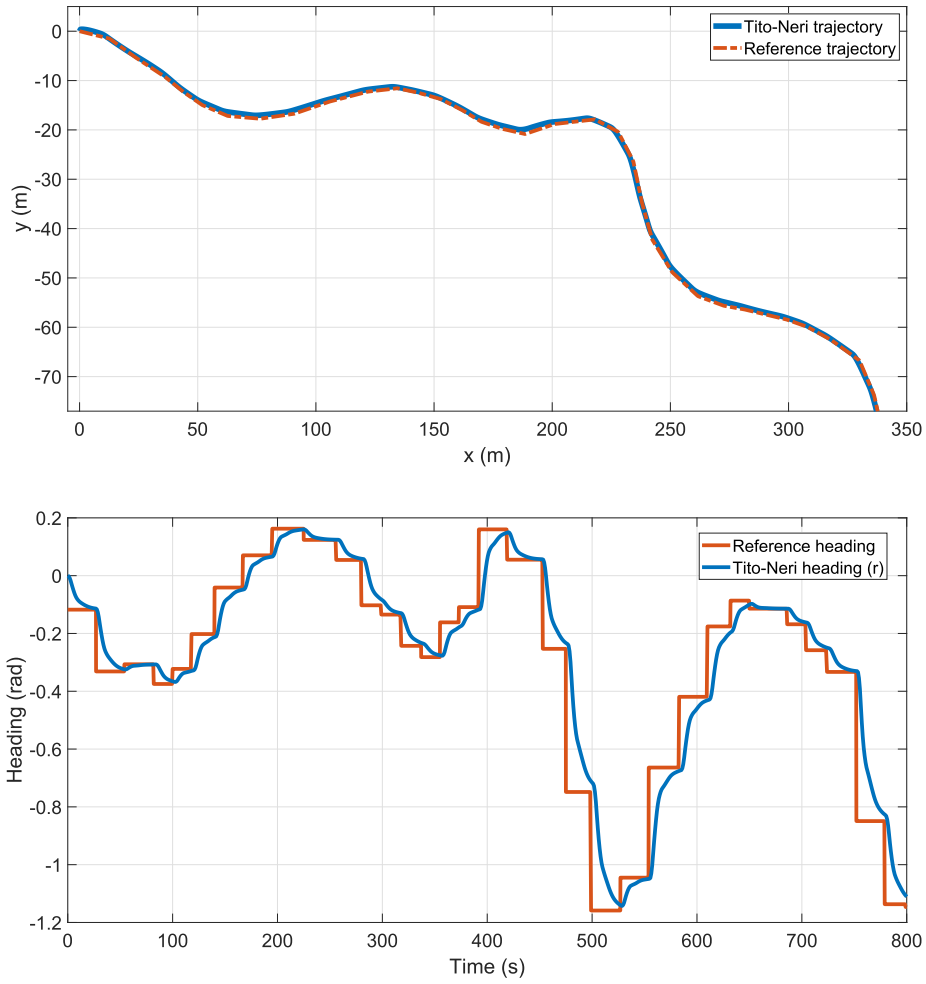

Fig. 18. Trajectory tracking simulation results in the port of Rotterdam (Experiment II).

that there is a current in the environment with $[-0.04, 0.05, 0]^T$ speed vector.

In this experiment, the proposed algorithm is compared with a MIMO nonlinear PID control scheme [23] where the control law is:

$$\tau = -K_{\mathrm{m}}\dot{V} + R^{-1}(\eta_{\mathrm{s}}(t))\tau_{\mathrm{PID}} \tag{71}$$

and

$$\tau_{\mathrm{PID}} = -K_{\mathrm{p}}(\eta_d - \eta) - K_{\mathrm{d}}\dot{\eta} - K_{\mathrm{i}}\int_0^t (\eta_d - \eta)d\tau. \tag{72}$$

Parameter K_{m} is the acceleration feedback. Other parameters are chosen as $K_{\mathrm{p}} = 0.8$, $K_{\mathrm{d}} = 1$ and $K_{\mathrm{m}} = 4$.

The experiment results are given in Fig. 7. Simulation results of trajectory tracking are compared in terms of Root-Square Error (RSE). From Fig. 7c, it can be inferred that by using the proposed methodology the ship can stay closer to the reference trajectory.

It is assumed that the real-size tug is under a pull force which increases over time. The simulation results of the energy consumption side are shown in Fig. 8. The bollard pull force increases from t = 300 s and it reaches to 420 kN after 620 s. As a result, the propelling effort increases which results in a higher shaft speed and electric torque of the propelling induction motors.

During this operation, it is assumed that the battery is in the charge mode which leads to higher load demands. The initial SOC is assumed to be 20%. The simulation results using the predictive energy management algorithm are provided in Figs. 9 and 10. The results indicate that despite of changes in the propulsive load, the optimal engine loading is achieved throughout the operation. In Figs. 11 and 12, the results related to the stability of the DC-PPS are given. The power share of each energy source determined by the energy management algorithm is provided in Fig. 11a. The voltage of the DC-link capacitor and speed of the diesel-generators are also provided which are stable around their desired values. The battery SOC and fuel consumption rate of the diesel engines are presented in Fig. 13 which indicate optimal loading consistency.

Experiment I is also carried out in battery discharge mode where the initial SOC is considered to be 80%. The simulation results in this case are shown in Fig. 14. Furthermore, the results are compared to a conventional Rule-Based (RB) strategy that is no energy source should provide more that 85% of its maximum deliverable power. The simulation results are provided in Figs. 15 and 16. It is observed that the optimal loading of the diesel engines cannot be achieved and the engine load varies during the operation. The results are provided in Table 1 for comparison. The results suggest that in this voyage, the SFC efficiency of the engines increases in charge and discharge modes if the proposed PEM approach is adopted. In the charging mode, the increase is 2.4% and in discharge mode it is 2.04%. Furthermore, using the proposed algorithm, the saved energy in the battery is more than three times higher.

6.2. Experiment II

In this experiment, the voyage of an inland vessel is extracted using AIS data of the Oude Maas river in the port of Rotterdam (Fig. 17). The trajectory is scaled down so that it is applicable to Tito-Neri vessel. This simulation is carried out twice, first using the proposed PEM algorithm

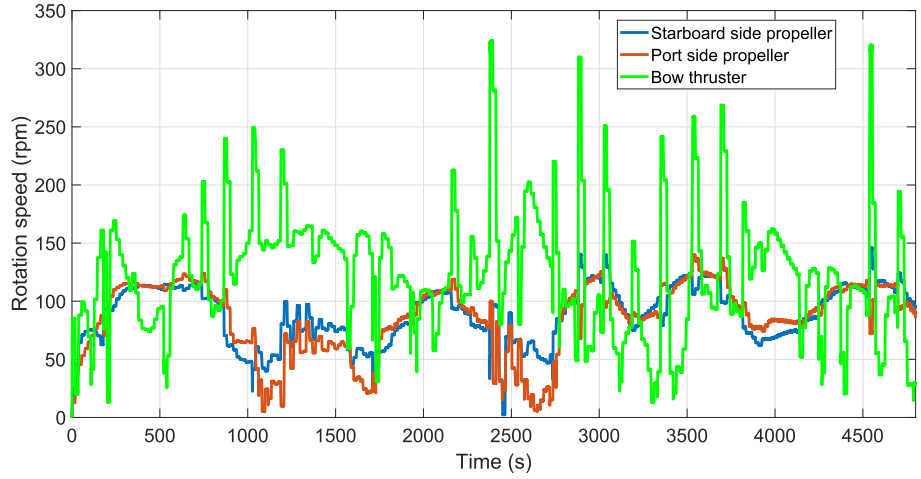

a) Shaft speed of propellers.

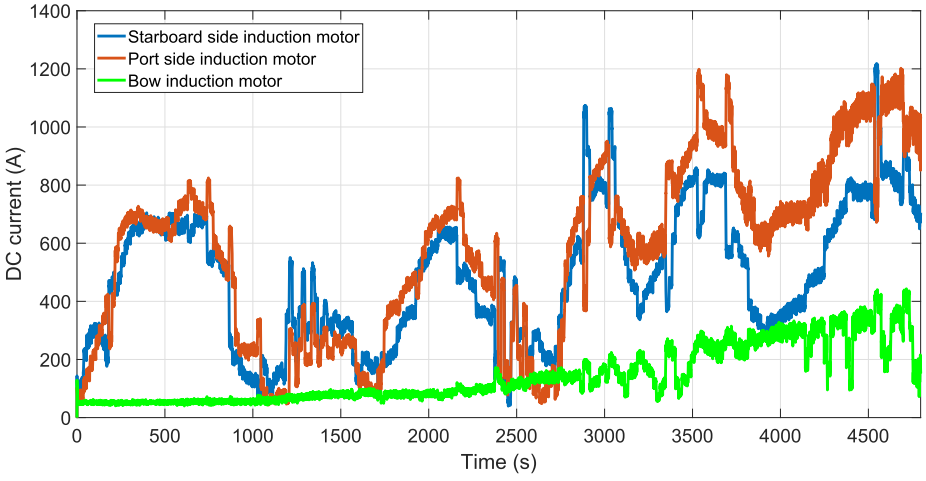

b) Input DC current of motor controller-inverters.

Fig. 19. Simulation results of propelling actuators (Experiment II).

and by adopting the conventional rule-based approach. In both cases, it is assumed that at the start of the simulation the battery SOC is at 20%. As a result, the battery is charged up to 80% of its capacity and then is used in discharge mode. In both cases, a full charge and discharge cycle is considered.

The results of the trajectory tracking are provided in Fig. 18. The shaft speed of the propelling actuators as well as the DC current of their motor-inverter controllers are shown in Fig. 19.

The simulation results of the energy generation side are shown in Figs. 20 and 21. It can be observed that a more optimal engine loading is achieved using the proposed energy management approach. The results are also presented in Table 2. The results indicate that using the proposed approach higher fuel efficiency can be achieved.

6.3. Experiment III

For the third experiment, the operating profile data of an actual harbor tug is used. There are four operating profiles, see Fig. 22 where the bollard pull force and the vessel speed are illustrated over the operation time. The operating profiles are different in terms of load fluctuation and power demand. Profile 1 is a standard profile based on measurements of tugboats in the port of Rotterdam. Profile 2 is a busy profile in which the vessel undergoes a heavy pull operation for relatively a long period. Profile 3 represents an operation where the load fluctuation is high. Profile 4 is an expansion of Profile 3 over time representing a busy profile with high load fluctuation.

The simulation results are provided in Table 3. For Profile I, although the fuel consumption is increased using the proposed energy management algorithm, the battery SOC reaches to 68%. This indicates that the available power is handled more efficiently. This can be confirmed by comparing the operation SFCs, where 12% SFC efficiency is obtained using the PEM approach. In the second profile, a complete charge and discharge cycle is not completed. However, the proposed approach offers 3.6% SFC efficiency. In the third profile also a complete cycle is not gained due to the short operation time. Using the proposed approach 3.8% and 4.4% SFC efficiency is gained in Profiles 3 and 4, respectively.

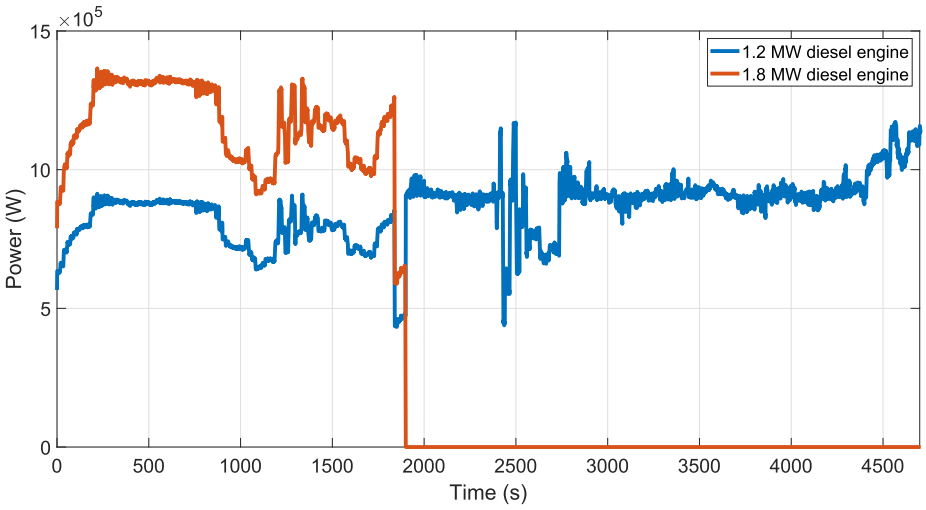

a) Generated power by diesel engines (PEM).

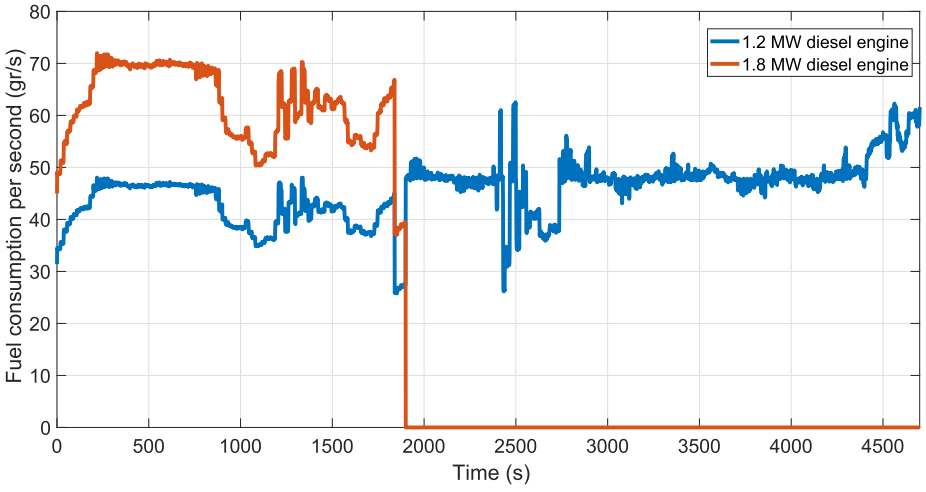

b) Fuel consumption rate (PEM).

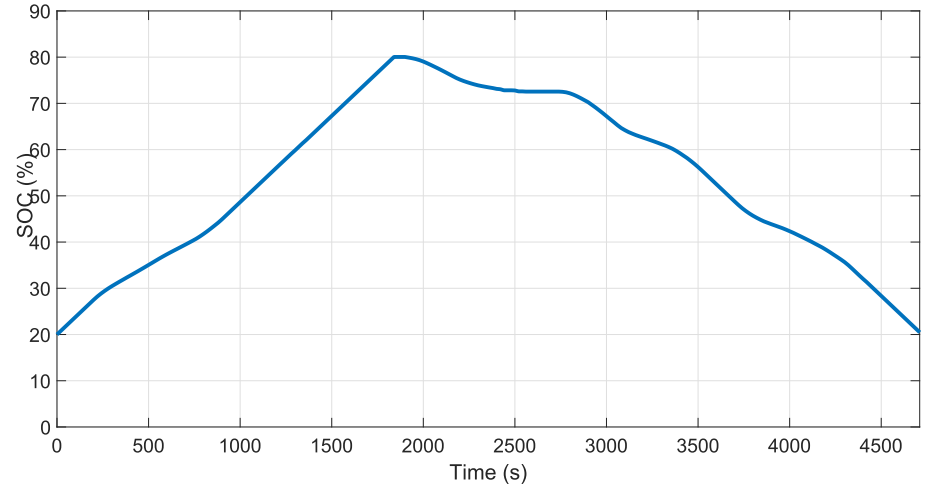

c) Battery SOC (PEM).

Fig. 20. Performance of the energy sources using PEM approach (Experiment II).

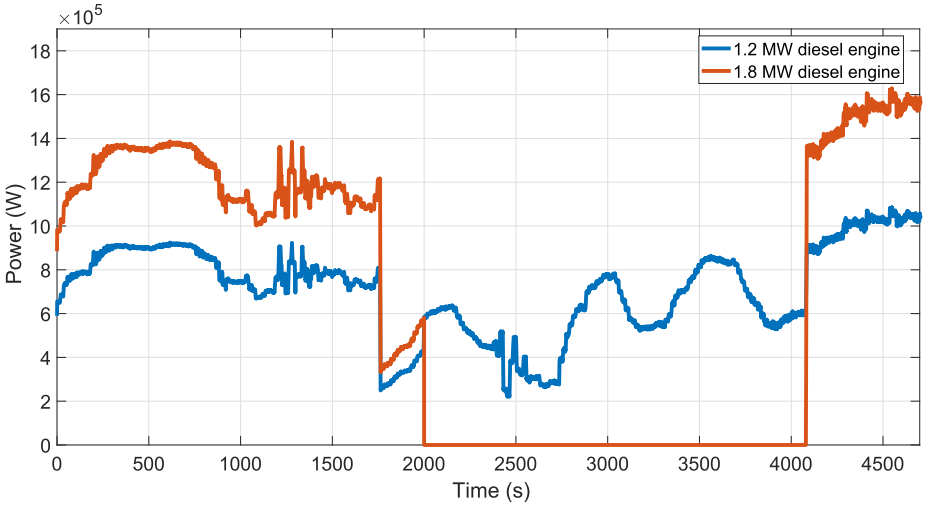

a) Generated power by diesel engines.

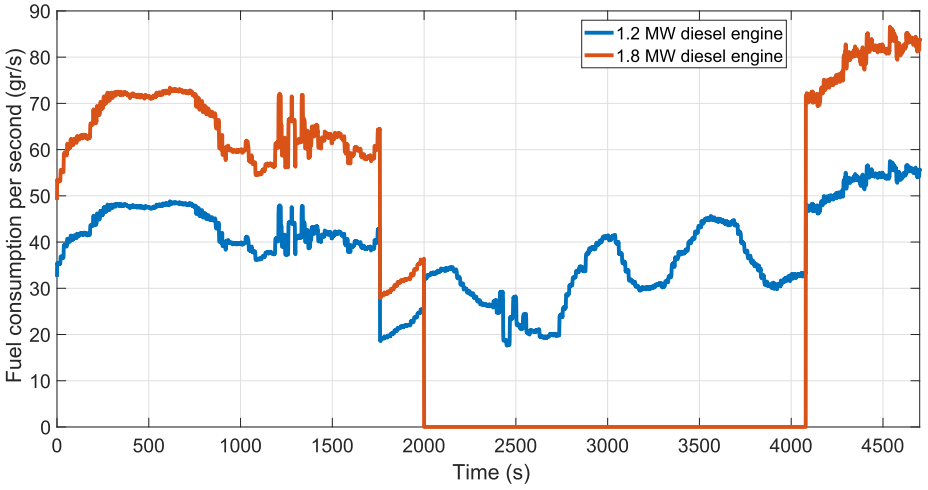

b) Fuel consumption rate.

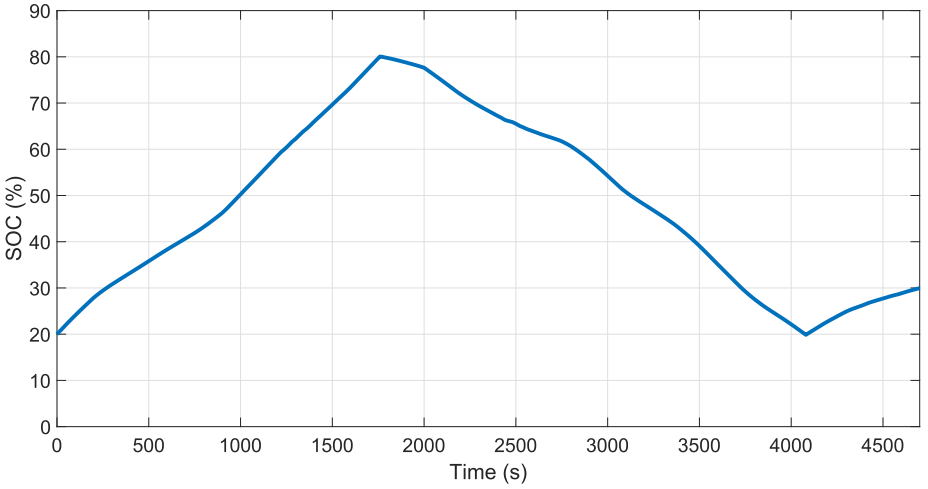

c) Battery SOC.

Fig. 21. Performance of the energy sources using the rule-based approach (Experiment II).

Table 2
Performance comparison of algorithms (Experiment II).

Algorithm	Fuel cons. (kg)	Mech. energy (kWh)	SFC
PEM	336.05	1753	191.7
RB	358.45	1842	194.6

7. Conclusions and future research

In this paper, a combination of model predictive approaches has been proposed for efficient voyage of autonomous electric ships. The focus of the paper has been on the all-electric Direct Current Power and Propulsion Systems (DC-PPS) in which the power system is a DC

Table 3
Simulation results of the operating profiles in Experiment III.

Profile	Algorithm	Start mode	Fuel cons. (kg)	Mech. en. (kWh)	SFC (gr/kWh)	No. of cycles	Final SOC (%)
I	RB	Charge	233.4	1062	219.7	1	20
I	PEM	Charge	282.2	1459	193.3	1	68
II	RB	Charge	808.2	4108	198.3	0	15
II	PEM	Charge	778	4068	191	0	17
III	RB	Discharge	151.2	751	201.4	0	32
III	PEM	Discharge	148.3	765	193.7	0	35
IV	RB	Charge	372.1	1801	206.2	1	33
IV	PEM	Charge	350.4	1772	197	1	31

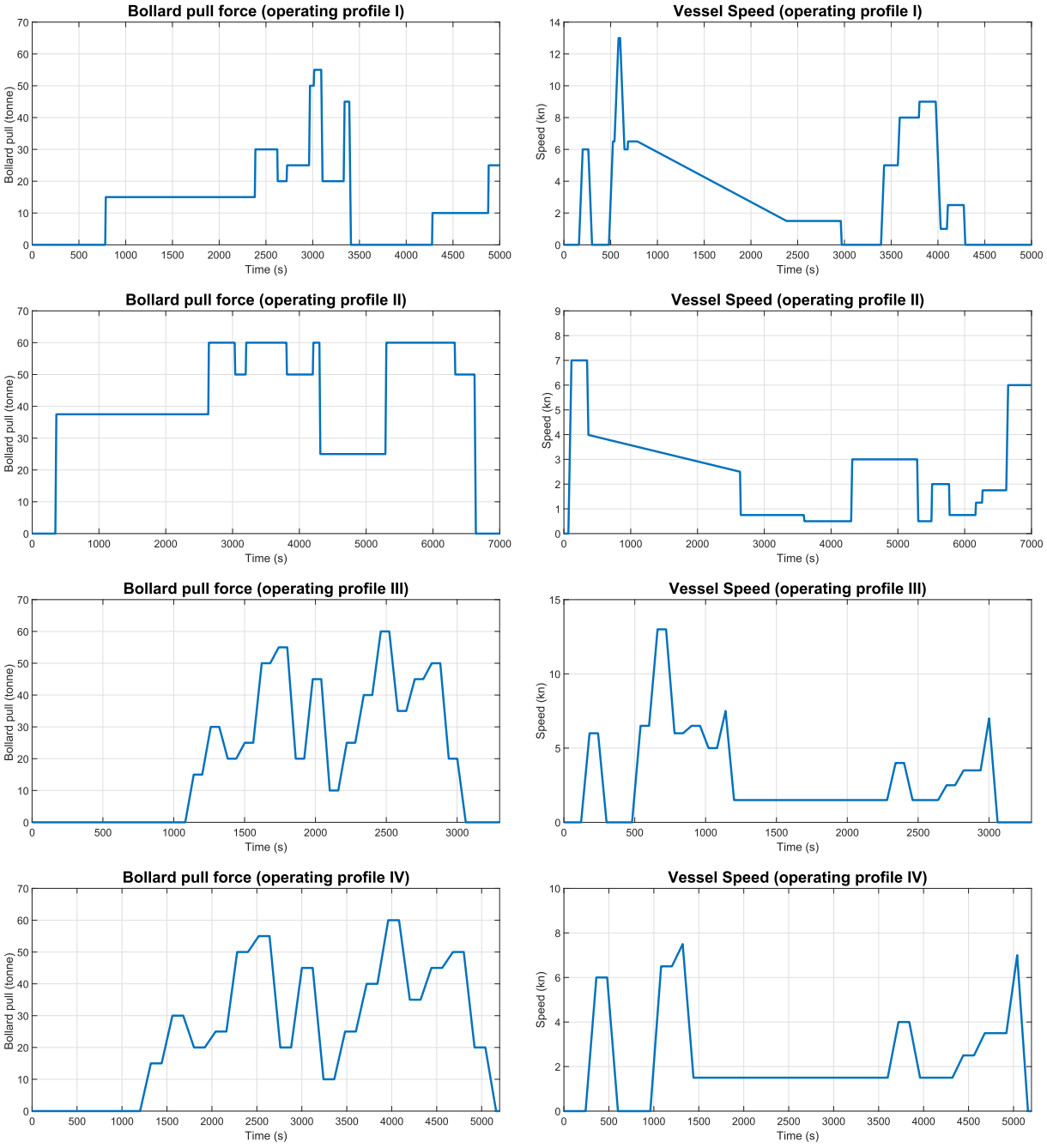

Fig. 22. Operating profiles (Experiment III).

microgrid. First, a maneuvering model for the autonomous ship in 3DoF has been presented. The DC-PPS has also been modeled and a dynamical model for every component has been presented. Then, a Model Predictive Control (MPC) algorithm has been proposed, designed using Input–Output Feedback Linearization (IOFL) and a constraint linearization technique so that quadratic programming approaches can be adopted for solving the optimization problem. Then, an energy management approach has been presented with which the optimal power split between different energy sources on-board of the vessel is determined. The algorithm incorporates the predictions of the maneuvering control algorithm as well as the Specific Fuel Consumption curve of diesel engines and battery model to address the fuel efficiency issue. The presented energy management approach can handle both charge and discharge modes of the battery and achieve a more efficient fuel consumption compared to conventional methods. For evaluating the performance of the presented approaches several simulation scenarios are considered. The simulation results indicate a decrease in trajectory tracking error, depending on the trajectory specifications and the environmental conditions. It is also shown that a significant efficiency can be obtained in fuel consumption. This research illustrates the viability of model predictive approaches for dealing with trajectory tracking as well as energy management issues in autonomous shipping.

After further evaluation by industrial communities, the proposed approaches can be adjusted and adopted for real applications. The proposed energy management approach can be implemented on the computer devices of the on-board energy management modules. The proposed maneuvering control scheme can be adopted for autopilot modes or dynamic positioning operations. It also can be used for futuristic applications such as autonomous sailing.

Future research should focus on making robust approaches to address the on-board power system stability problems [8]. Furthermore, uncertainties should be taken into account. The uncertainties can be the result of environmental disturbances as well as modeling mismatches. Adaptive control approaches should be combined with MPC approaches to deal with the problem of uncertainty in maneuvering control and predicting the future required power. The results of this paper can also be extended to the domain of controlling multiple autonomous ships which could lead to more efficient platoons and vessel train formations [7].

Acknowledgments

The authors thank the Port of Rotterdam Authority for providing the AIS data of the ship trajectory in Section 6.2 and Daan de Boer for categorizing and arranging the data. The authors also thank the R&D department of Damen Shipyard Gorinchem for providing the operating profiles in Section 6.3. The Tito-Neri maneuvering model has been extracted by Daan Bruiggink, Quintin Cremer, Rik Groenewegen and Aernout Klokgieters under the supervision of Vittorio Garofano, Ali Haseltalab, and Rudy R. Negenborn. All are affiliated with Delft University of Technology.

This research is supported by the project “ShipDrive: A Novel Methodology for Integrated Modelling, Control, and Optimization of Hybrid Ship Systems” (project 13276) of the Netherlands Organisation for Scientific Research (NWO), domain Applied and Engineering Sciences (TTW).

Appendix A. Maneuvering model of Tito-Neri

The parameters of the maneuvering model are provided in Table A.4. The drag forces are estimated using the graphs in Fig. 23. Moreover, $\tau_{\text{drag}_\theta} = \frac{l}{3}\tau_{\text{drag}_y}\left(\frac{\pi}{2}, \frac{2v_r}{3}\right)$. For more information regarding the Tito-Neri model, see [39].

Table A.4
Maneuvering model parameters.

Parameter	Symbol	Value	Unit
Mass of the ship	m_b	16.9	kg
Mass matrix	M_{RB}	$\begin{bmatrix} 16.9 & 0 & 0 \\ 0 & 16.9 & 0 \\ 0 & 0 & 0.51 \end{bmatrix}$	$\begin{bmatrix} \text{kg} \\ \text{kg} \\ \text{kg}\times\text{m}^2 \end{bmatrix}$
Added mass matrix	M_A	$\begin{bmatrix} 1.2 & 0 & 0 \\ 0 & 49.2 & 0 \\ 0 & 0 & 1.8 \end{bmatrix}$	$\begin{bmatrix} \text{kg} \\ \text{kg} \\ \text{kg}\times\text{m}^2 \end{bmatrix}$
Length of the ship	l	0.97	m
Width of the ship	w	0.3	m
Center of gravity	CoG	$\begin{bmatrix} 0 \\ 0 \end{bmatrix}$	$\begin{bmatrix} \text{m} \\ \text{m} \end{bmatrix}$
Port thruster location	–	$\begin{bmatrix} -0.42 \\ -0.08 \end{bmatrix}$	$\begin{bmatrix} \text{m} \\ \text{m} \end{bmatrix}$
Starboard thruster location	–	$\begin{bmatrix} -0.42 \\ 0.08 \end{bmatrix}$	$\begin{bmatrix} \text{m} \\ \text{m} \end{bmatrix}$

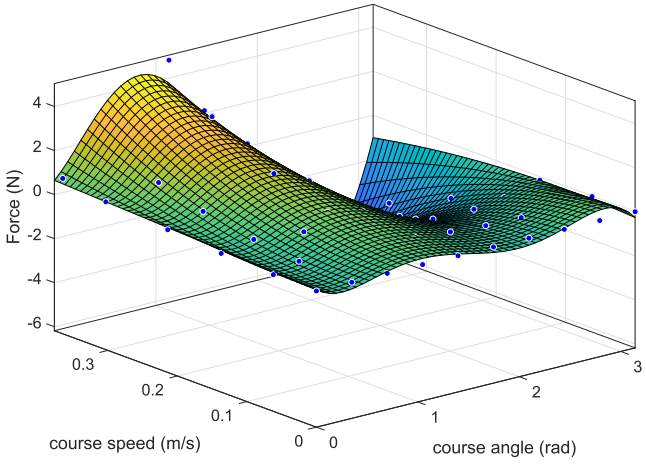

(a) Longitudinal drag forces in the body-fixed frame.

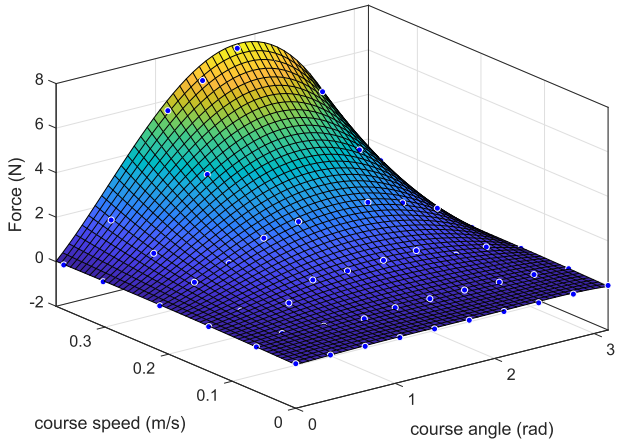

(b) Lateral drag forces in the body-fixed frame.

Fig. 23. The graph of Tito-Neri drag forces.

Appendix B. Specifications of the PPS

B.1. Diesel engine

I. 1.8 MW DGR set: $K_{en} = 2.2 \times 10^4$, rated speed: 188.5 rad/s, $a = 6.45 \times 10^7$ gr.kWh, $b = 3.45 \times 10^{-5}$ gr/kWh^2, $c = 96.21$ gr/kWh.
II. 1.2 MW DGR set: $K_{en} = 1.4 \times 10^4$, rated speed: 188.5 rad/s, $a = 3.68 \times 10^7$ gr.kWh, $b = 4.40 \times 10^{-5}$ gr/kWh^2, $c = 109.60$gr/kWh.

B.2. Synchronous generators

I. 1.8 MW DGR set: 1.8 MW, 460 v, 60 Hz, 4 poles, $J = 112.8$, $r_s = 0.0008$, $r_{fd} = [0.00015$, $r_{kd} = 0.016$, $r_{kq} = 0.0021$, $L_d = 0.0077$, $L_{md} = 1.273 \times 10^{-5}$, $L_{kd} = 0.00054$, $L_{fd} = 8.7 \times 10^{-5}$, $L_q = 0.00052$, $L_{mq} = 0.00051$ and $L_{kq} = 5.2 \times 10^{-5}$.
II. 1.2 MW DGR set: 1.2 MW, 460 v, 60 Hz, 4 poles, $J = 96.4$, $r_s = 0.0011$, $r_{fd} = 0.00045$, $r_{kd} = 0.034$, $r_{kq} = 0.0041$, $L_d = 0.012$, $L_{md} = 0.00014$, $L_{kd} = 0.0011$, $L_{fd} = 0.0017$, $L_q = 0.00091$, $L_{mq} = 0.0013$ and $L_{kq} = 0.00013$.

Resistance values are in ohms and inductance values are in Henry.

B.3. Rectifier

Snubber values of six-pulse rectifiers, $r_{sn} = 100$ ohms and $C_{sn} = 1e - 5$ F.

B.4. DC-Link

$C = 0.05$ F.

B.5. Induction motor

I. Induction motors of propellers: 1.5 MW, 460 v, 60 Hz, 4 poles, $J_m = 4.2$, $r_{sm} = 0.0001818$, $r_{rm} = 0.0009956$, $L_{sm} = 0.00099$, $L_{mm} = 0.0009415$, $L_{rm} = 0.00096$.
II. Induction motor of the bow thruster: 0.5 MW, 460 v, 60 Hz, 4 poles, $J_m = 3.1$, $r_{sm} = 0.0148$, $r_{rm} = 0.00929$, $L_{sm} = 0.0108$, $L_{mm} = 0.0104$, $L_{rm} = 0.0105$.

Resistance values are in ohms and inductance values are in Henry. Direct torque control is used for the control of induction motors [Krause, P. C. Analysis of Electric Machinery. New York: McGraw-Hill, 1986.].

B.6. Propelling actuators

I. Propellers: $K_T = 0.59$, $K_Q = 0.046$, $D = 2.4$ m, $\rho = 1024 kg/m^2$.
II. Bow thruster: $K_T = 0.56$, $K_Q = 0.041$, $D = 1$ m, $\rho = 1024 kg/m^2$.

B.7. Battery

$C_n = 2000$ Ah, $\eta_i = 0.96$ (charge mode), $v_b = 400$ V.

B.8. Bidirectional converter

$C_c = 267\,\mu$F, $L_c = 516\,\mu$H, $R_c = 19$ ohm, $n = 3$.

References

[1] Hassani V, Lande SV. Path planning for marine vehicles using Bézier curves. In: Proceedings of 11th IFAC conference on control applications in marine systems (CAMS). Opatija, Croatia; 2018.
[2] Bitar G, Breivik M, Lekkas AM. Energy-optimized path planning for autonomous ferries. In: Proceedings of 11th IFAC conference on control applications in marine systems (CAMS). Opatija, Croatia; 2018.
[3] Zheng H, Negenborn RR, Lodewijks G. Predictive path following with arrival time awareness for waterborne AGVs. Transport Res Part C: Emerg Technol 2016;70:214–37.
[4] Haseltalab A, Negenborn RR. Adaptive control for a class of partially unknown non-affine systems: applied to autonomous surface vessels. In: Proceedings of 20th IFAC World Congress. Toulouse, France; 2017. p. 4252–7.
[5] Zheng H, Negenborn RR, Lodewijks G. Fast ADMM for distributed model predictive control of cooperative waterborne AGVs. IEEE Trans Control Syst Technol 2017;25(4):1406–13.
[6] Zheng H, Negenborn RR, Lodewijks G. Robust distributed predictive control of waterborne AGVs –a cooperative and cost-effective approach. IEEE Trans Cybernet 2018;48(8):2449–61.
[7] Chen L, Hopman JJ, Negenborn RR. Distributed model predictive control for vessel train formations of cooperative multi-vessel systems. Transport Res Part C: Emerg Technol 2018;92:101–18.
[8] Geertsma R, Negenborn RR, Visser K, Hopman J. Design and control of hybrid power and propulsion systems for smart ships: a review of developments. Appl Energy 2017;194:30–54.
[9] Kalikatzarakis M, Geertsma R, Boonen E, Visser K, Negenborn RR. Ship energy management for hybrid propulsion and power supply with shore charging. Control Eng Practice 2018;76:133–54.
[10] Hou J, Song Z, Park H, Hofmann H, Sun J. Implementation and evaluation of real-time model predictive control for load fluctuations mitigation in all-electric ship propulsion systems. Appl Energy 2018;230:62–77.
[11] Babaei M, Shi J, Abdelwahed S. A survey on fault detection, isolation, and re-configuration methods in electric ship power systems. IEEE Access 2018;6:9430–41.
[12] Li W, Monti A, Ponci F. Fault detection and classification in medium voltage dc shipboard power systems with wavelets and artificial neural networks. IEEE Trans Instrument Measur 2014;63(11):2651–65.
[13] Zhou J, Yang Y, Zhao Z, Ding SX. A fault detection scheme for ship propulsion systems using randomized algorithm techniques. Control Eng Practice 2018;81:65–72.
[14] Geertsma R, Visser K, Negenborn RR. Adaptive pitch control for ships with diesel mechanical and hybrid propulsion. Appl Energy 2018;228:2490–509.
[15] Zahedi B, Norum L. Modeling and simulation of all-electric ships with low-voltage DC hybrid power systems. IEEE Trans Power Electron 2013;28(10):4525–37.
[16] Haseltalab A, Negenborn RR. Predictive on-board power management for all-electric ships with DC distribution architecture. In: Proceedings of OCEANS 2017 – Aberdeen; 2017. p. 1–8.
[17] Zahedi B, Norum LE, Ludvigsen KB. Optimized efficiency of all-electric ships by DC hybrid power systems. J Power Sour 2014;255:341–54.
[18] Haseltalab A, Botto MA, Negenborn RR. On-board voltage regulation for all-electric dc ships. IFAC-PapersOnLine 2018;51(29):341–7. in Proceedings of 11th IFAC Conference on Control Applications in Marine Systems, Robotics, and Vehicles CAMS 2018.
[19] Hou J, Sun J, Hofmann H. Adaptive model predictive control with propulsion load estimation and prediction for all-electric ship energy management. Energy 2018;150:877–89.
[20] Abdelaal M, Fränzle M, Hahn A. Nonlinear model predictive control for trajectory tracking and collision avoidance of underactuated vessels with disturbances. Ocean Eng 2018;160:168–80.
[21] Park BS. Adaptive formation control of underactuated autonomous underwater vehicles. Ocean Eng 2015;96:1–7.
[22] Skjetne R, Smogeli YN, Fossen TI. A nonlinear ship manoeuvering model: identification and adaptive control with experiments for a model ship. Model, Identif Control 2004;25(1):3–27.
[23] Fossen TI. Handbook of marine craft hydrodynamics and motion control. West Sussex (UK): Wiley; 2011.
[24] Dai S, Wang M, Wang C. Neural learning control of marine surface vessels with guaranteed transient tracking performance. IEEE Trans Indust Electron 2016;63(3):1717–27.
[25] Zhao Z, He W, Ge SS. Adaptive neural network control of a fully actuated marine surface vessel with multiple output constraints. IEEE Trans Control Syst Technol 2014;22(4):1536–43.
[26] Zheng H, Negenborn RR, Lodewijks G. Closed-loop scheduling and control of waterborne agvs for energy-efficient inter terminal transport. Transport Res Part E: Logist Transport Rev 2017;105:261–78.
[27] Kurtz MJ, Henson MA. Input-output linearizing control of constrained nonlinear processes. J Process Control 1997;7(1):3–17.
[28] ter Braake HAB, Botto MA, van Can HJL, da Costa JS, Verbruggen HB. Linear predictive control based on approximate input-output feedback linearisation. IEE Proc - Control Theory Appl 1999;146(4):295–300.
[29] Izadi-Zamanabadi R, Blanke M. A ship propulsion system as a benchmark for fault-tolerant control. Control Eng Practice 1999;7(2):227–39.
[30] Barnitsas D, Ray MM, Kinley P. Kt, kq and efficiency curves for the wageningen b-series propellers, Tech. rep., Department of Naval Architecture and Marine Engineering, University of Michigan, Ann Arbor; 1981.
[31] Krause PC, Wasynczuk O, Pekarek S. Analysis of electric machinery and drive systems. 3rd ed. Wiley; 2013.
[32] Grimmelius P, Schulten HT, Stapersma D. The use of diesel engine simulation models in ship propulsion plant design and operation. In: Proceedings of CIMAC; 2007.
[33] Geertsma R, Negenborn RR, Visser K, Loonstijn M, Hopman J. Pitch control for ships with diesel mechanical and hybrid propulsion: modelling, validation and performance quantification. Appl Energy 2017:1609–31.
[34] Blanke M, Andersen J. On dynamics of large two stroke diesel engines. New Res Identif 1984.
[35] Smogeli ON. Control of marine propellers Ph.D. thesis Norwegian University of Science and Technology; 2006.
[36] Jatskevich J, Pekarek SD, Davoudi A. Parametric average-value model of synchronous machine-rectifier systems. IEEE Trans Energy Convers 2006;21(1):9–18.
[37] Plett GL. Extended Kalman filtering for battery management systems of LiPb-based HEV battery packs: Part 1. Background. J Power Sour 2004;134(2):252–61.
[38] Syverud TH. Modeling and control of a DC-grid hybrid power system with battery and variable speed diesel generators [Master's thesis]; 2016.
[39] Bruggink DJJB, Cremer QC, Groenewegen RR, Klokgieters AGC. Differentiation of maneuvering coefficients for scaled model vessels; 2018.